Table F–10. Calibrated horizontal hydraulic-conductivity parameters for the volcanic-rock units.

[BRU, Belted Range unit; CFBCU, Crater Flat–Bullfrog confining unit; CFPPA, Crater Flat–Prow Pass aquifer; CFTA, Crater Flat–Tram aquifer; CHVU, Calico Hills volcanic-rock unit; LFU, lava-flow unit; OVU, older volcanic-rock unit; PVA, Paintbrush volcanic-rock aquifer; SWNVF, southwestern Nevada volcanic field; TMVA, Thirsty Canyon–Timber Mountain volcanic-rock aquifer]

Parameter name	Description	Minimum – maximum hydraulic conductivity, in meters per day, from Belcher and others, 2001	Composite scaled sensitivity	Hydraulic conductivity at land surface (meters per day)	Coefficient of variation[1]	Average depth (meters)	Hydraulic conductivity at average depth (meters per day)
K311 YVU (lumped with part of CHVU; K32BR4CH13)							
K312 LFU (part lumped with VSU (upper); K42UP_VSU)							
K3LFU_am	LFU in Amargosa Desert area	0.002–4	0.0904	5.094×10^{-2}	0.23	38	0.0410
K3C_TM	TMVA - brittle (either altered or not)	[3]2×10^{-4}–20	1.029	8.440	0.5	144	3.71
K3211TMVA	TMVA - not brittle (either altered or not)	[3]2×10^{-4}–20	0.280	5.662×10^{-1}	0.44	588	0.197
K3C_PVA	Intracaldera PVA	[2]7×10^{-7}–17	0.08808	0.3162	NA	248	0.0767
K3PVA	Extra-caldera PVA	[2]7×10^{-7}–17	0.2820	2.885×10^{2}	[11]0.29	248	70.00
K32CH24LF	(1) CHVU – altered, brittle (2) CHVU – not altered, not brittle (3) LFU – all areas except Amargosa Desert	[4]0.002–4	0.1776	1.328×10^{-1}	0.42	[12]38	0.107
K32BR4CH13	(1) BRU – not brittle, not altered (2) WVU (3) CHVU – not altered, brittle (4) CHVU – altered, not brittle	[5]0.008–4	0.2840	1.604×10^{-1}	0.11	[13]175	0.05917
K321521_PP	CFPPA	[6]0.001–180	0.5710	1.661×10^{2}	0.5	693	3.183
K3215BCU1	CFBCU – not altered, brittle	[6]0.001–180	0.04711	1.000×10^{-2}	0.26	561	0.000406
K3215BCU34	CFBCU – not brittle (either altered or not)	[7]0.0003–55	0.3780	1.241	0.49	562	0.05012
K3215TR	CFTA	[8]0.003–2	0.1347	5.597×10^{-2}	0.49	721	0.000914
K3BRU123	(1) BRU – not altered, brittle (2) BRU – altered, brittle (3) BRU – altered, not brittle	[9]0.01–4	0.1597	1.894	0.5	561	0.07693
K33_OVU	OVU outside SWNVF	[10]1×10^{-6}–1	0.01341	9.900×10^{-3}	0.021	142	0.004388
K33_OVUsw	OVU inside SWNVF	[10]1×10^{-6}–1	0.1867	4.8638×10^{-2}	0.061	509	0.002658

[1]Values were log transformed.

[2]Range listed is for the PVA.

[3]Range listed is for the TMVA.

[4]Range listed is for the LFU, which includes the range of the CHVU.

[5]Minimum value listed is for CHVU and the maximum value listed is for the BRU.

[6]Range listed is for the CFPPA.

[7]Range listed is for the CFBCU.

[8]Range listed is for the CFTA.

[9]Range listed is for the BRU.

[10]Range listed is for the OVU.

[11]Parameter was not log transformed.

[12]Average depth is for the LFU, the most spatially extensive unit.

[13]Average depth is for the BRU, the most spatially extensive unit.

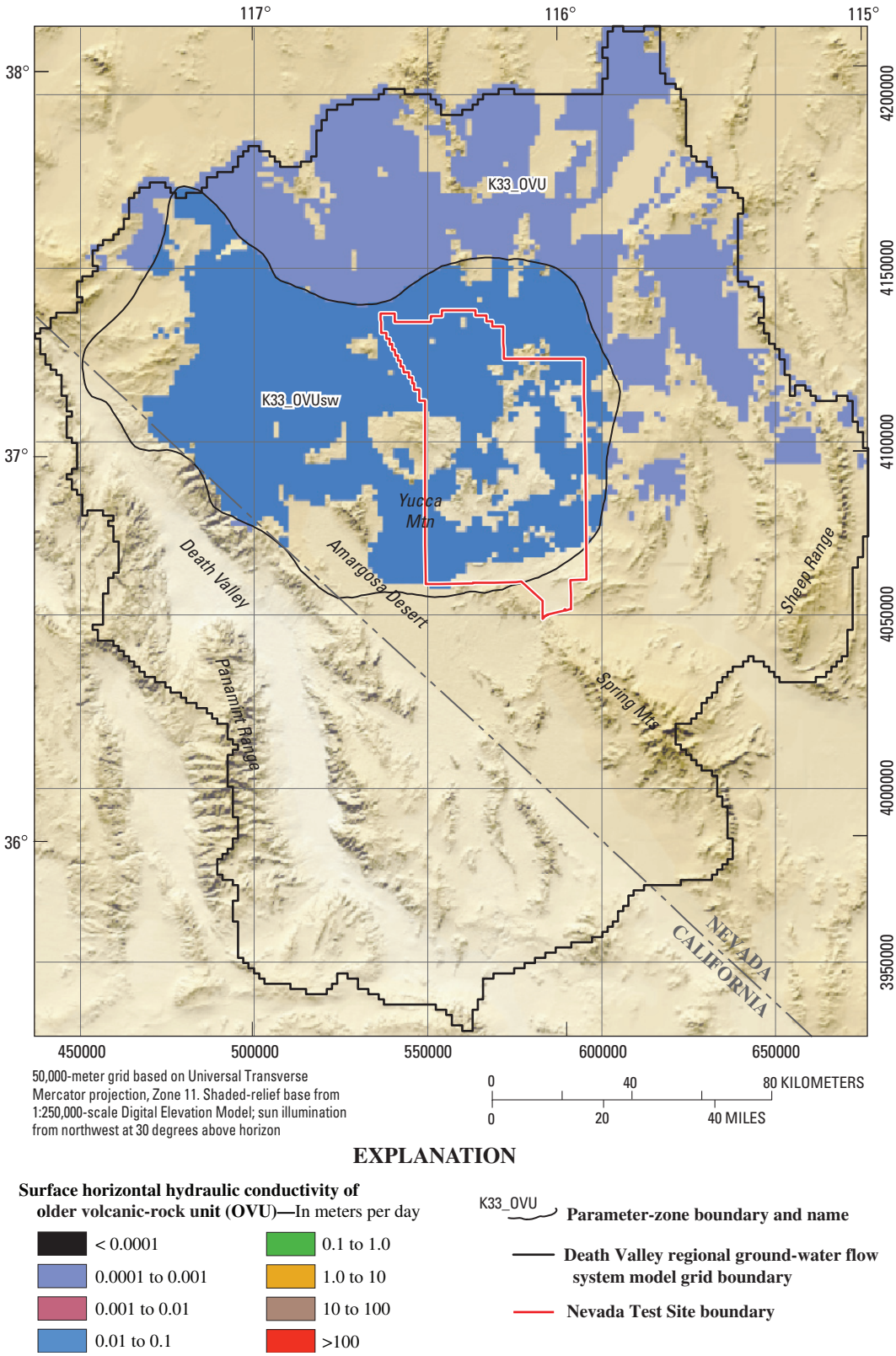

Figure F–19. Hydraulic-conductivity zone parameters, unit thickness, and extent for older volcanic-rock unit.

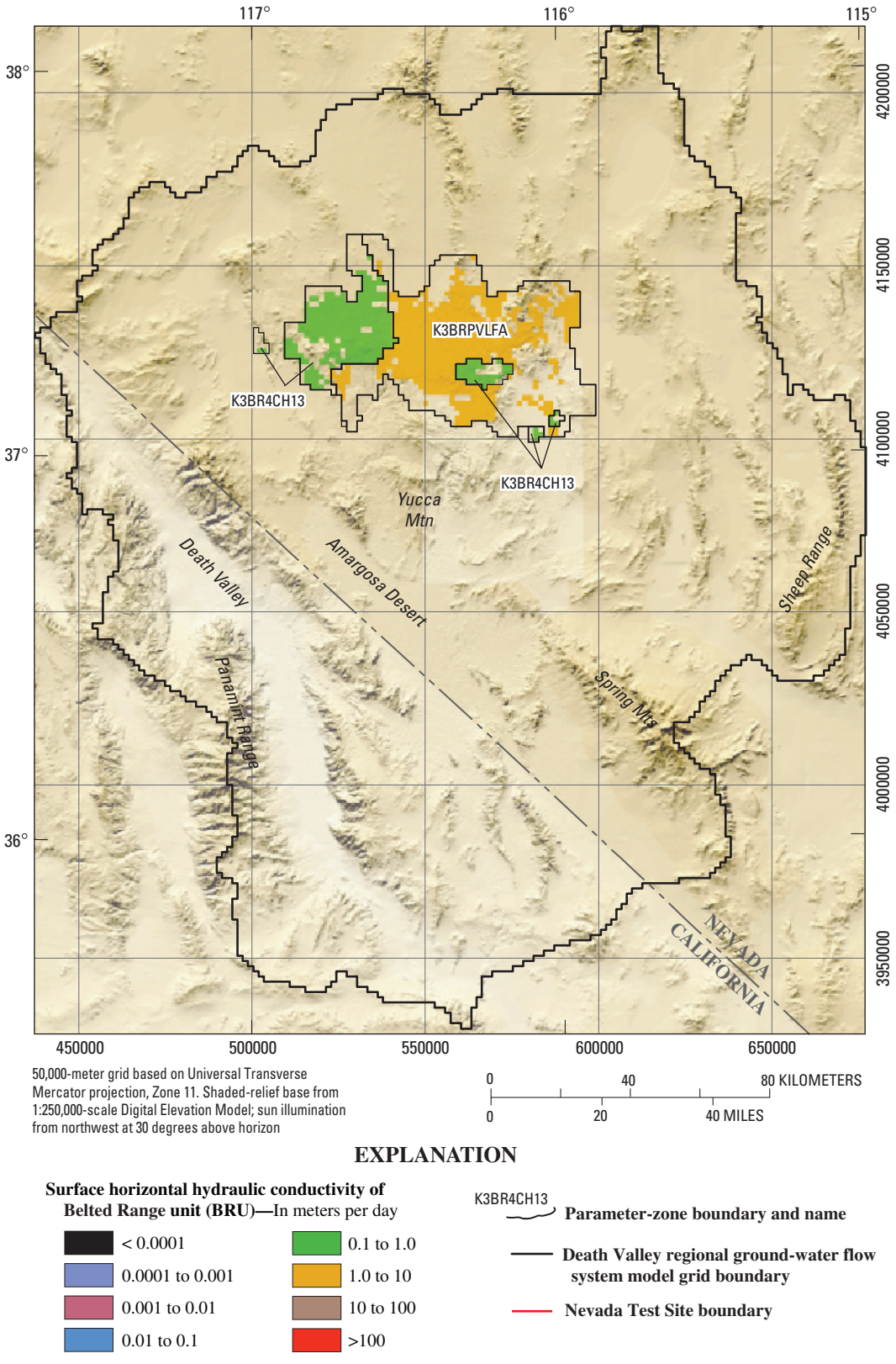

Figure F–20. Hydraulic-conductivity zone parameters, unit thickness, and extent for belted Range unit.

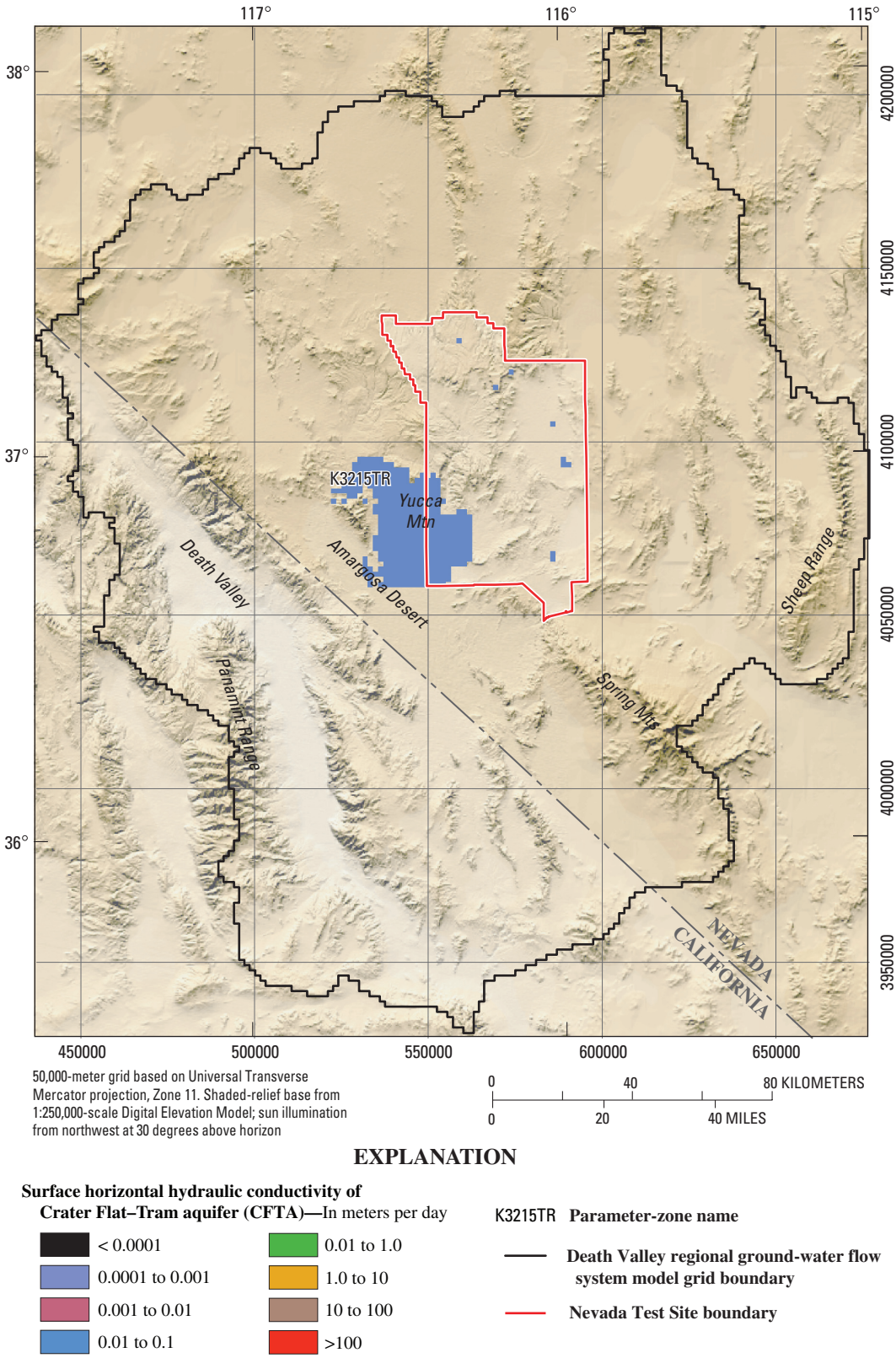

Figure F–21. Hydraulic-conductivity zone parameters, unit thickness, and extent for Crater Flat–Tram aquifer unit.

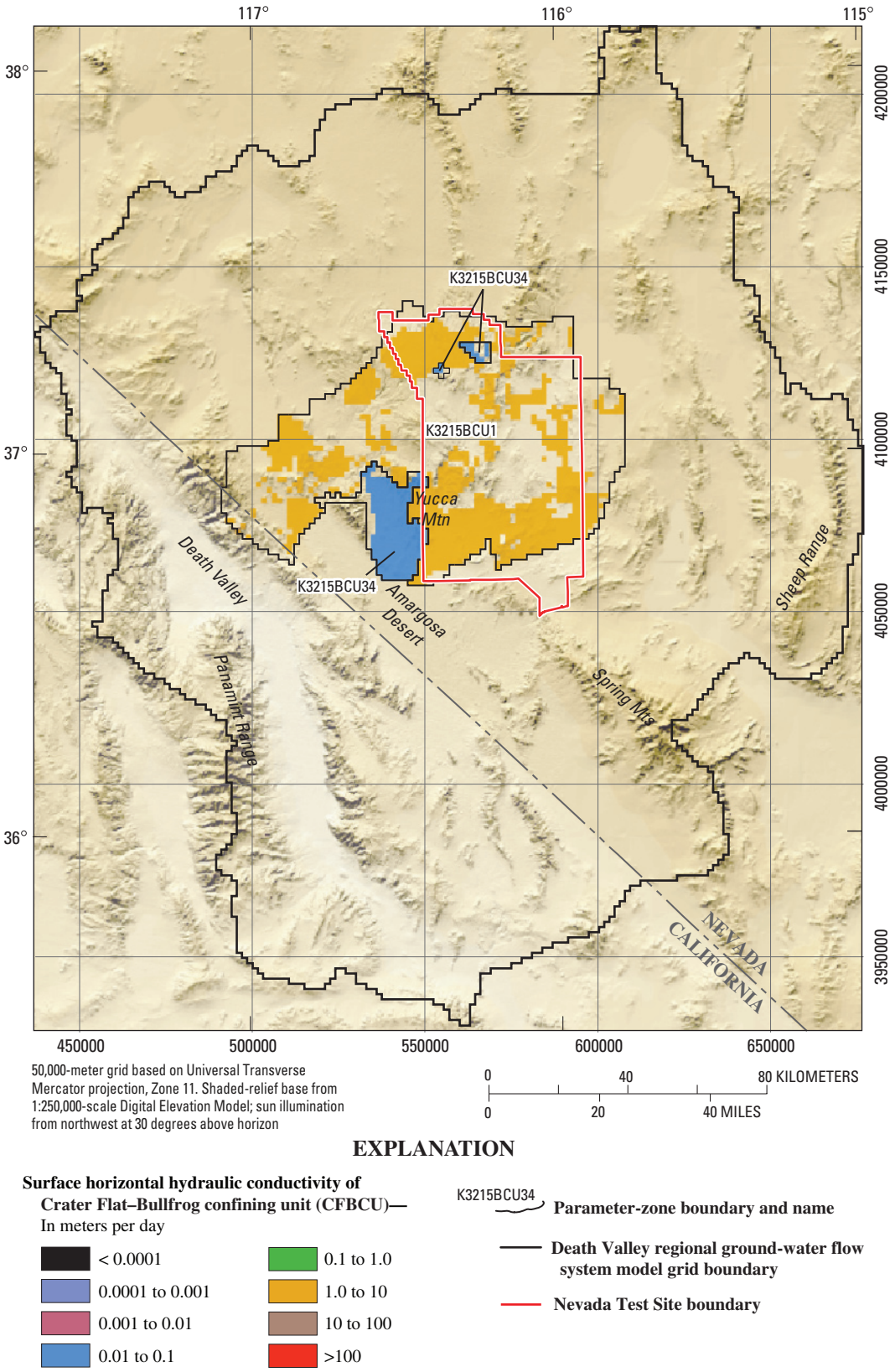

Figure F–22. Hydraulic-conductivity zone parameters, unit thickness, and extent for Crater Flat–Bullfrog confining unit.

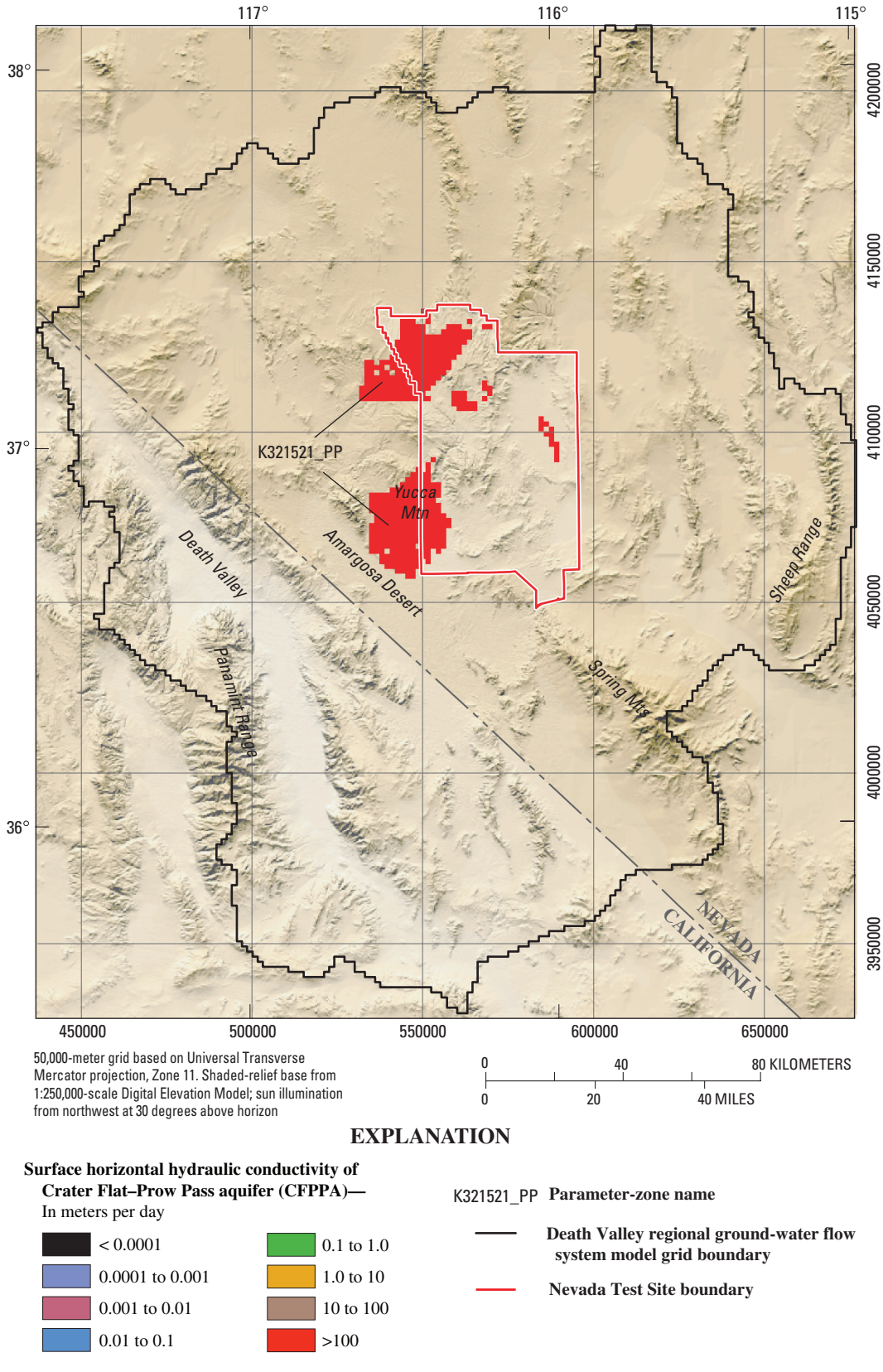

Figure F–23. Hydraulic-conductivity zone parameters, unit thickness, and extent for Crater Flat–Prow Pass aquifer unit.

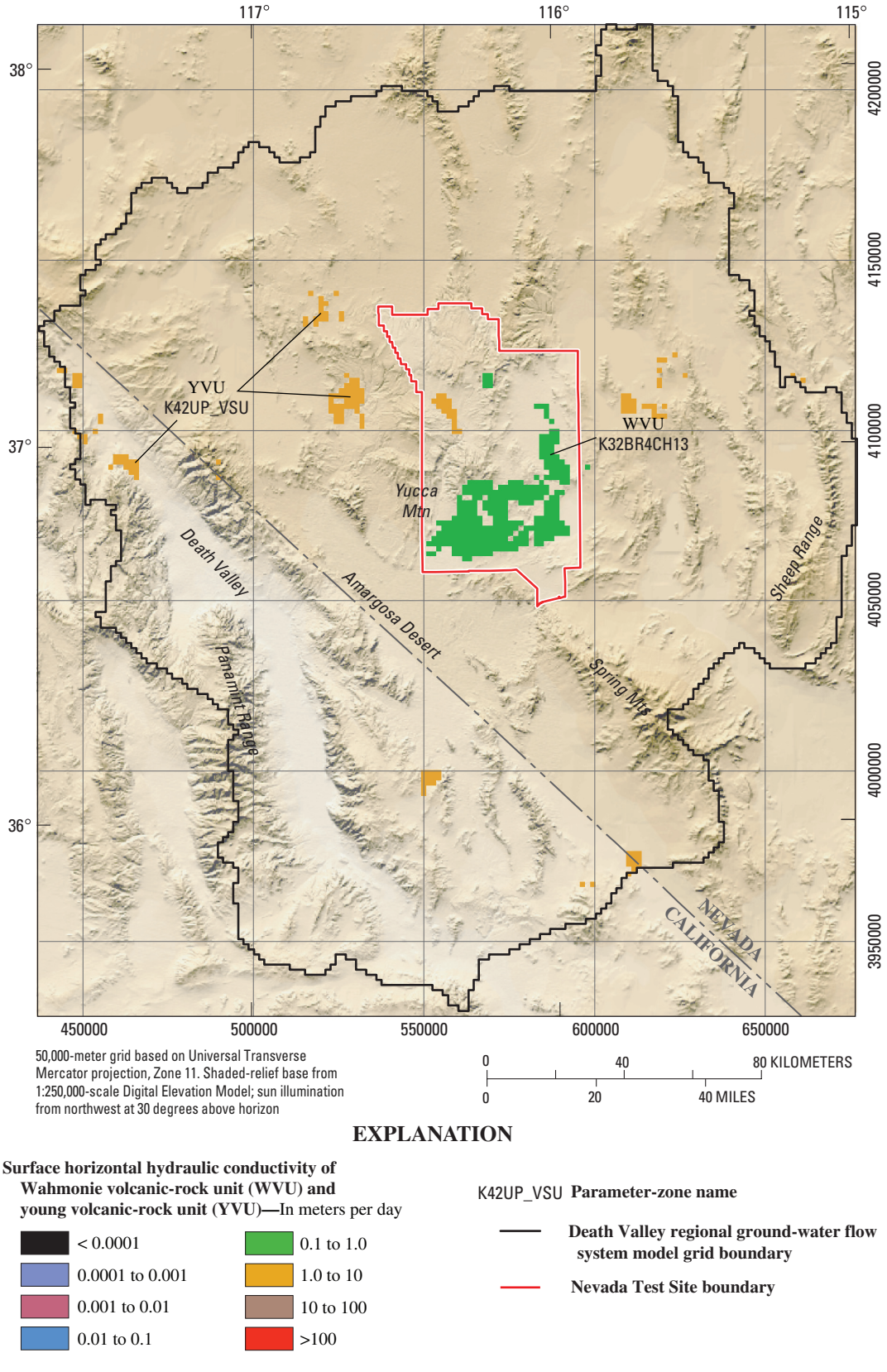

Figure F–24. Hydraulic-conductivity zone parameters, unit thickness, and extent for Wahmonie volcanic-rock and younger volcanic-rock unit.

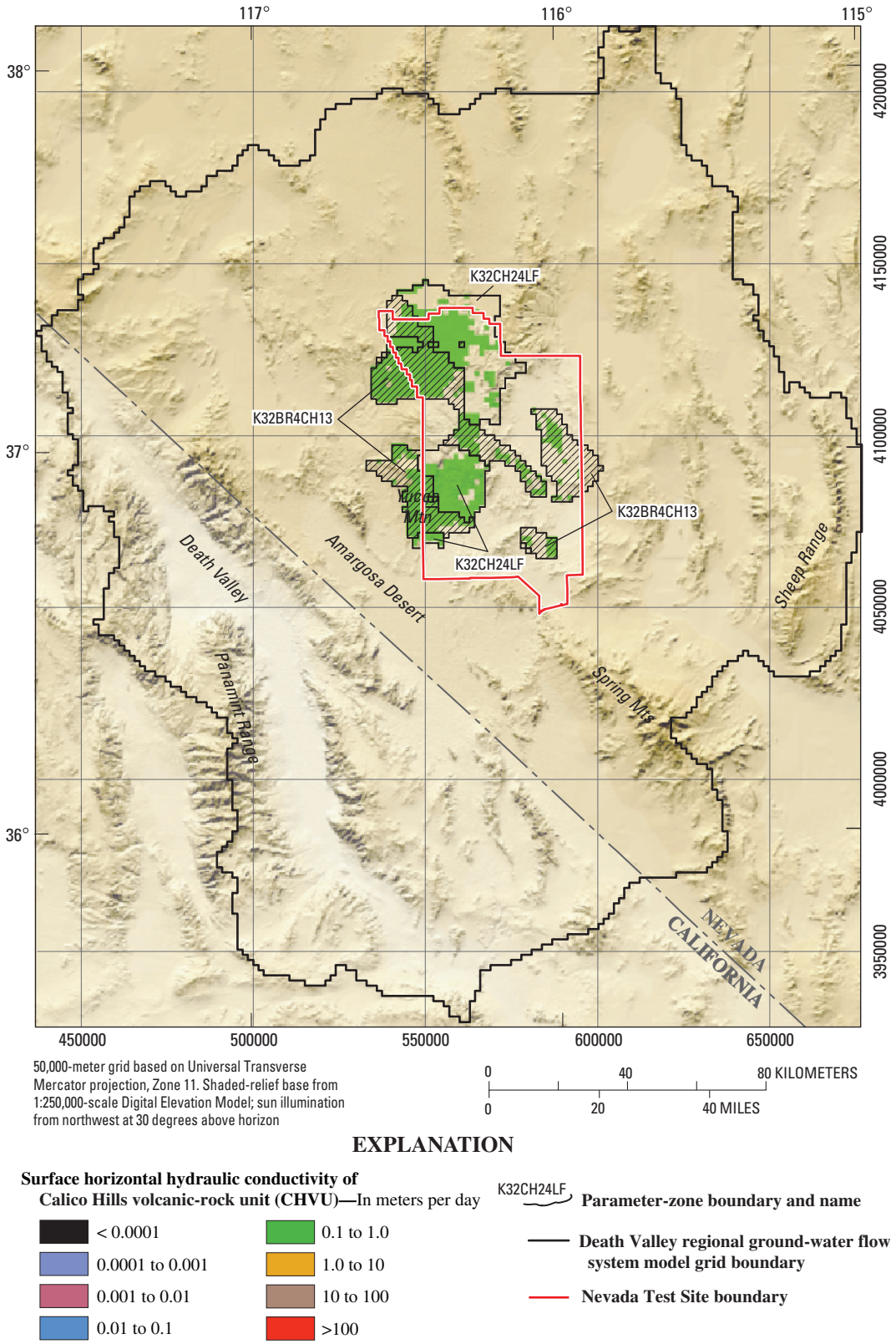

Figure F–25. Hydraulic-conductivity zone parameters, unit thickness, and extent for Calico Hills volcanic-rock unit.

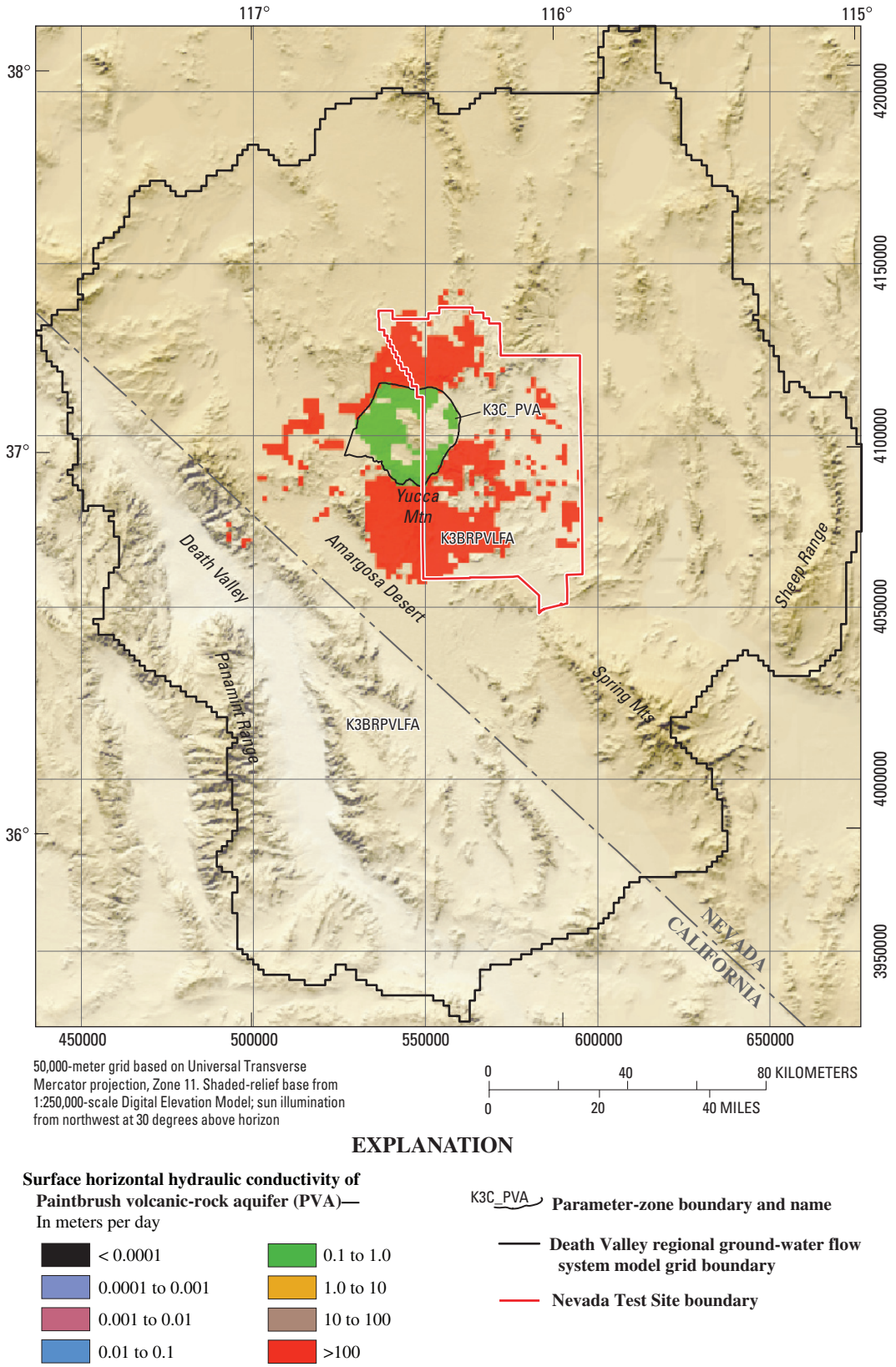

Figure F–26. Hydraulic-conductivity zone parameters, unit thickness, and extent for Paintbrush volcanic-rock aquifer.

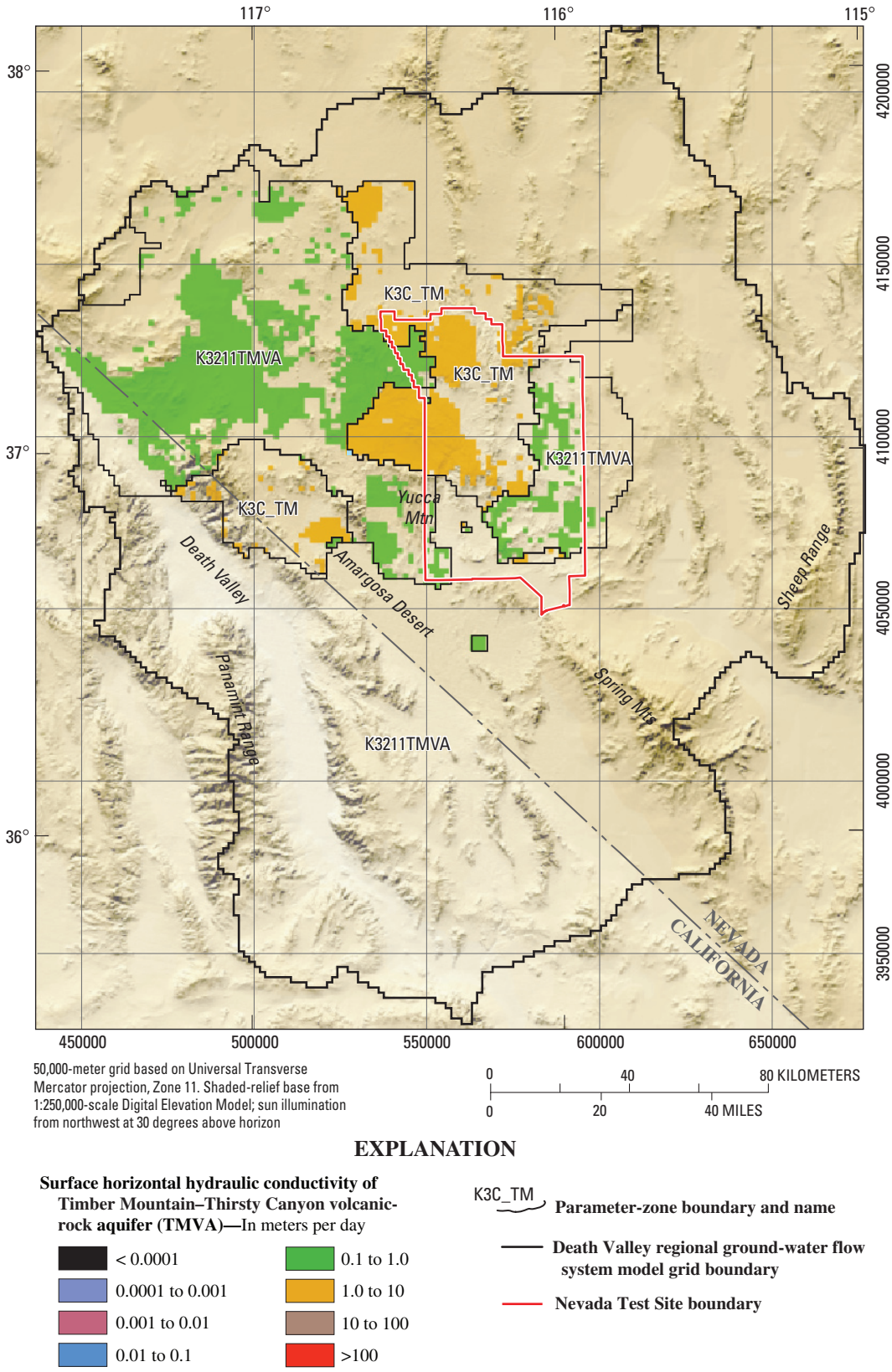

Figure F–27. Hydraulic-conductivity zone parameters, unit thickness, and extent for Thirsty Canyon–Timber Mountain volcanic-rock aquifer.

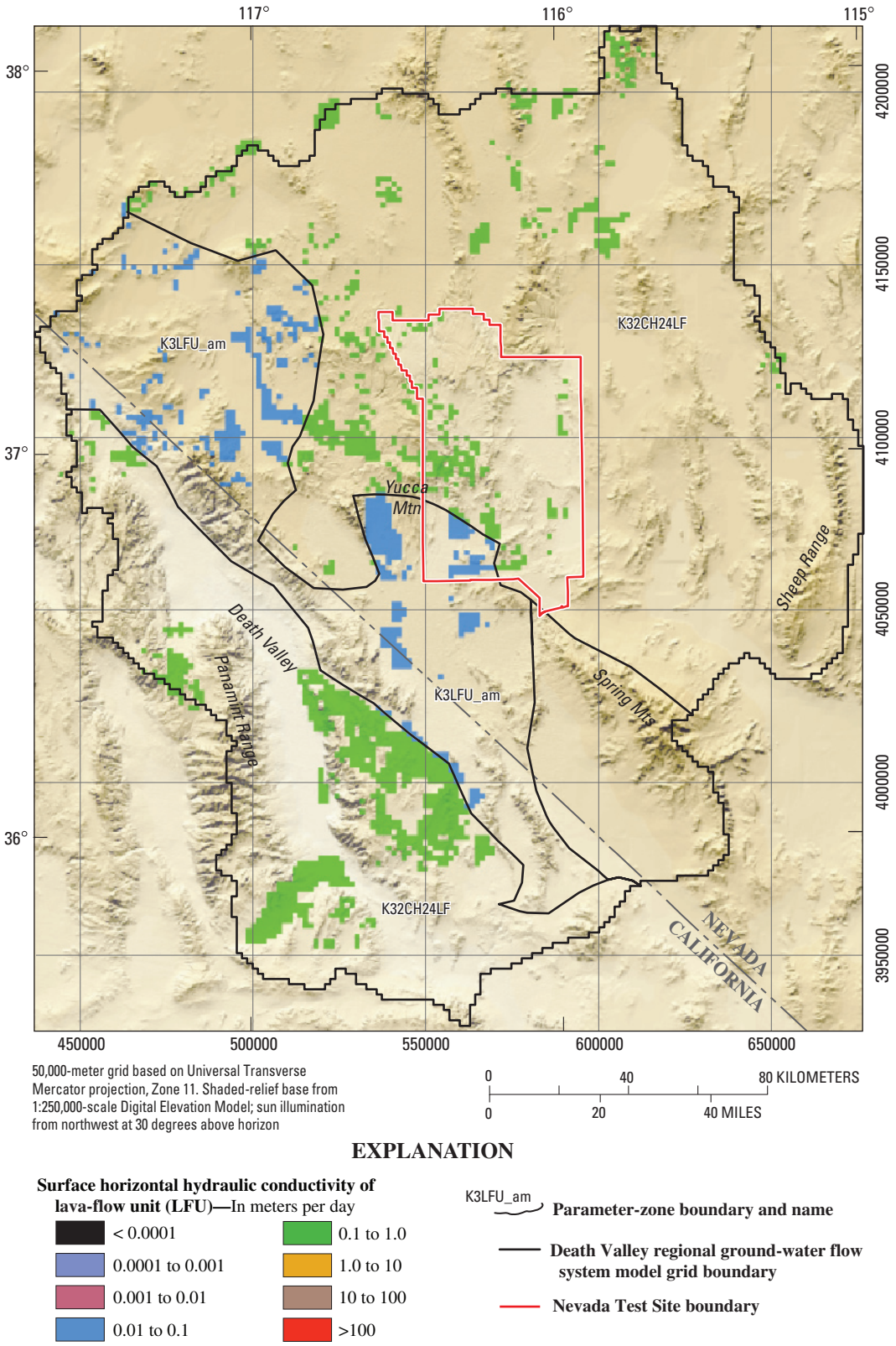

Figure F–28. Hydraulic-conductivity zone parameters, unit thickness, and extent for lava-flow unit.

Some volcanic HGUs, such as the WVU, did not have enough hydraulic information to subdivide into zones and thus were left intact and commonly combined with other HGUs. In one case, that of the PVA, the property zonations did not appear to support the hydraulic data at all. The PVA was divided on the basis of its relative location inside or outside caldera centers (fig. F–26), which likely coincides with fracture density.

Basin-Fill Units

The HGUs constituting the basin-fill units were initially grouped into one hydraulic-conductivity parameter (K4). These units were initially split into two hydraulic-conductivity parameters representing aquifers (YAA, LA, and OAA) and confining units (YACU, OACU, and upper and lower VSU (table F–11)). The upper and lower VSUs were assigned into a parameter defining units that tend to be confining units even though they can be both confining units and aquifers.

Because the upper and lower VSUs can represent both aquifers and confining units, they were split on the basis of depositional characteristics of the basins. Hydraulic-conductivity zone parameters for these basin-fill units were defined on the basis of facies (figs. F–29 and F–30). The lower VSU was initially subdivided by facies (Chapter B, this volume). During calibration, this unit was further subdivided, especially in Pahrump Valley (fig. F–29). The basin-fill deposits in Pahrump Valley likely are more carbonate-rich and possibly of different character. The playa deposits in Pahrump Valley contain large amounts of fine-grained clays typical of a dry playa. The lower VSU also was important for matching heads and discharges near Sarcobatus Flat (fig. F–29) and flow in from the constant-head boundary (Clayton and the western part of Stone Cabin–Railroad boundary segments) (fig. A2–3 in Appendix 2). As a result, the lower VSU section representing the SWNVF sediments was split into an SWNVF area and a northeast and northwest component (fig. F–29 and table F–11).

The upper VSU was zoned on the basis of the location of the YACU and OACU because these relatively low permeability, fine-grained deposits were assumed to persist through time. This resulted in parameter zones (K4UP_VSUC, K4UP_VSUP, and K42UP_VSU) with similar depositional environments (fig. F–30 and table F–11).

The upper part of the basin-fill deposits is composed of a sequence of older and younger deposits defined by grain size. The older basin-fill are composed of the OACU (fig. F–31) and the OAA (fig. F–32), whereas the younger basin-fill units are composed of the YACU (fig. F–33) and the YAA (fig. F–34). The coarse-grained deposits are represented by the YAA and OAA (and fine-grained deposits represented by the YACU and OACU. Localized limestone aquifers in the basin-fill deposits were represented by the LA, which was combined into the hydraulic-conductivity parameter representing basin-fill aquifers (K4_VF_AQ). During calibration, these units were lumped and split as necessary.

Parameter zones also were used to assess the importance of the lower and upper VSU units in controlling ground-water discharge (figs. F–29—F–30 and table F–11). The YACU and finer grained parts of the VSUs limit the flow of ground water to discharge areas and pumping centers, especially near Ash Meadows and in Pahrump Valley.

CSS values of many of the basin-fill units are much larger in the transient calibration than in the steady-state calibration. Additional parameters were created in the basin-fill units and the lower and upper VSU to discern confining units and aquifers (figs. F–29—F–34 and table F–11). Specific storage parameters and hydraulic conductivities were adjusted by examining the simulated and observed changes in both discharge and hydraulic-head observations over time.

Depth Decay of Hydraulic Conductivity

Depth decay of hydraulic conductivity was simulated using the HUF package (Anderman and Hill, 2003) (table F–12 and fig. F–35). Because of the uncertainty in depth decay of hydraulic conductivity and the great effect this can have on model calibration, the initial parameter values were inserted on the basis of previous estimates of hydraulic-conductivity decay with depth (IT Corporation, 1996, figs. 6–1—6–3). In general, depth decay was important in all of the volcanic-rock units, all of the basin-fill units, and of somewhat lesser importance in the carbonate-rock aquifer, as indicated by IT Corporation (1996). Depth decay applied to zones within the LCCU, SCU, XCU, and ICU confining units was helpful for improving the model. Initially, depth decay of hydraulic conductivity was assigned to all areas of the carbonate-rock aquifer. In some areas, depth decay reduced model fit and made calibrations less than optimal. In these areas, the rate of decrease in hydraulic conductivity with depth was reduced. Although this change is subjective, it improved model fit.

Depth decay produces some values of hydraulic-conductivity that are outside expected values. This may indicate that values of the depth-decay parameters are in error or that the decay of hydraulic conductivity with depth is not an exponential function (eq. 1). In addition, hydraulic-conductivity values become extremely small at depth for many of the units (table F–12). In reality, the hydraulic conductivity may not decrease below a certain threshold value. The flow system can be simulated adequately without this parameter. Because depth-decay of hydraulic conductivity is more important in simulating the contaminant migration than ground-water flow, transport simulations could be helpful to quantify this value.

Table F–11. Calibrated horizontal hydraulic-conductivity parameters for the basin-fill units.

[Abbreviations: LA, limestone aquifer; OAA, older alluvial aquifer; OACU, older alluvial confining unit; SCU, sedimentary-rock confining unit; VSU, volcanic- and sedimentary-rock units; YAA, younger alluvial aquifer; YACU, younger alluvial confining unit; YVU, younger volcanic-rock unit]

Parameter name	Description	Minimum – maximum hydraulic conductivity (meters per day) from Belcher and others (2001)	Composite scaled sensitivity	Hydraulic conductivity at land surface (meters per day)	Coefficient of variation[1]	Average depth (meters)	Hydraulic conductivity at average depth (meters per day)
K4_VF_AQ	(1) Basin-fill aquifers (coarser grained) (LA, YAA) (2) SCU	[1]6×10^{-5}–130	0.342	5.972×10^{-1}	0.5	10	0.4467
K4_VF_OAA	OAA	[1]6×10^{-5}–130	0.0349	5.920×10^{-2}	0.5	39	0.000197
K4_VF_CU	Basin-fill confining units (finer grained) (YACU, OACU)	[2]0.003–34	0.547	1.580	0.5	43	0.4655
K4UP_VSUC	Upper VSU (below YACU or OACU); finer grained	[4]0.00004–6	0.578	9.397×10^{-1}	0.13	164	0.18256
K4UP_VSUP	Upper VSU (below YACU) in Pahrump Valley; finer grained	[4]0.00004–6	0.253	$2.077\text{x}10^{1}$	0.5	160	4.169
K42UP_VSU	(1) Upper VSU ; coarser grained (anywhere not below YACU or OACU) (2) YVU	[4]0.00004–6	0.572	7.057	0.5	159	1.438
K42222_VSU	Lower VSU; mixture of fluvial and lacustrine sediments (LCCU-derived, nonvolcanic, and finer grained sediments); small area of Amargosa Desert added during calibration	[4]0.00004–6	0.130	5.000×10^{-3}	0.01	401	0.004476
K422LNEVSU	Lower VSU; SWNVF sediments – northeast	[4]0.00004–6	0.311	1.847×10^{-1}	0.0001	721	0.15135
K422LNWVSU	Lower VSU; SWNVF sediments – northwest	[4]0.00004–6	0.770	1.917×10^{-1}	0.04	1,144	0.1397
K4222S_VSU	Lower VSU; SWNVF sediments	[4]0.00004–6	0.927	1.264×10^{-1}	0.06	1,296	0.088357
K422DV_VSU	Lower VSU; coarse syntectonic sediments (nonvolcanic) in Death Valley	[4]0.00004–6	0.399	8.804×10^{-3}	0.02	608	0.007442
K422GW_VSU	Lower VSU; Greenwater volcanic sediments	[4]0.00004–6	1.078	1.524×10^{-2}	0.003	572	0.013008
K4222P_VSU	Lower VSU; fluvial and lacustrine sediments with few volcanic units in Pahrump Valley	[4]0.00004–6	0.0866	5.812×10^{-1}	0.5	601	0.49227
K422GV_VSU	Lower VSU; mixture of sediments with diverse lithologies in the Amargosa Desert area	[4]0.00004–6	0.325	4.630×10^{-2}	0.02	689	0.038276

[1]Values were log transformed.

[2]Range listed is for the alluvial aquifer (AA), which is the combined YAA and OAA and includes the range of the SCU.

[3]Range listed is for the alluvial confining unit (ACU), which is the combined YACU and OACU.

[4]Range listed is for the combined YVU/VSU.

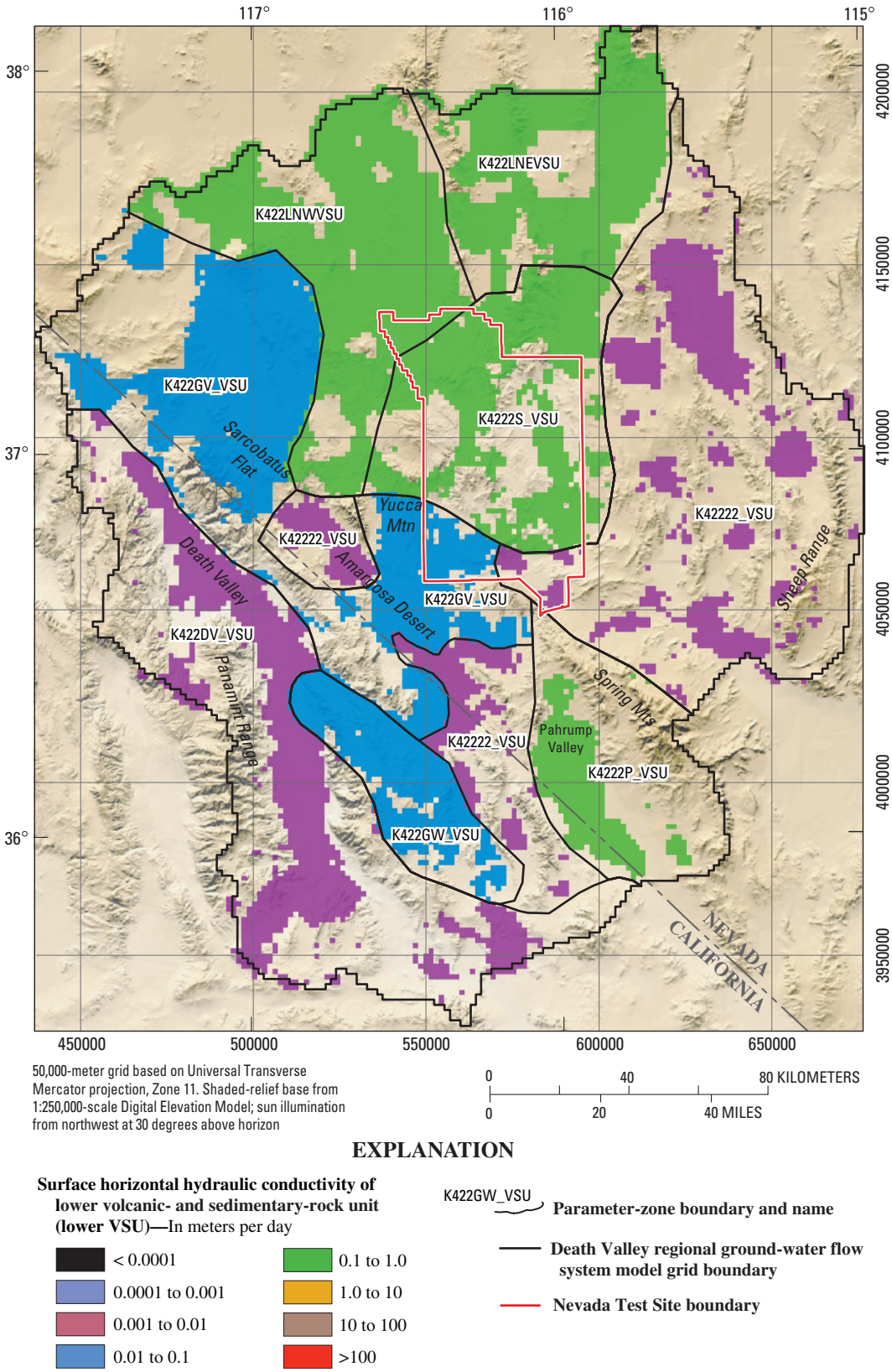

Figure F–29. Hydraulic-conductivity zone parameters, unit thickness, and extent for lower volcanic- and sedimentary-rock unit.

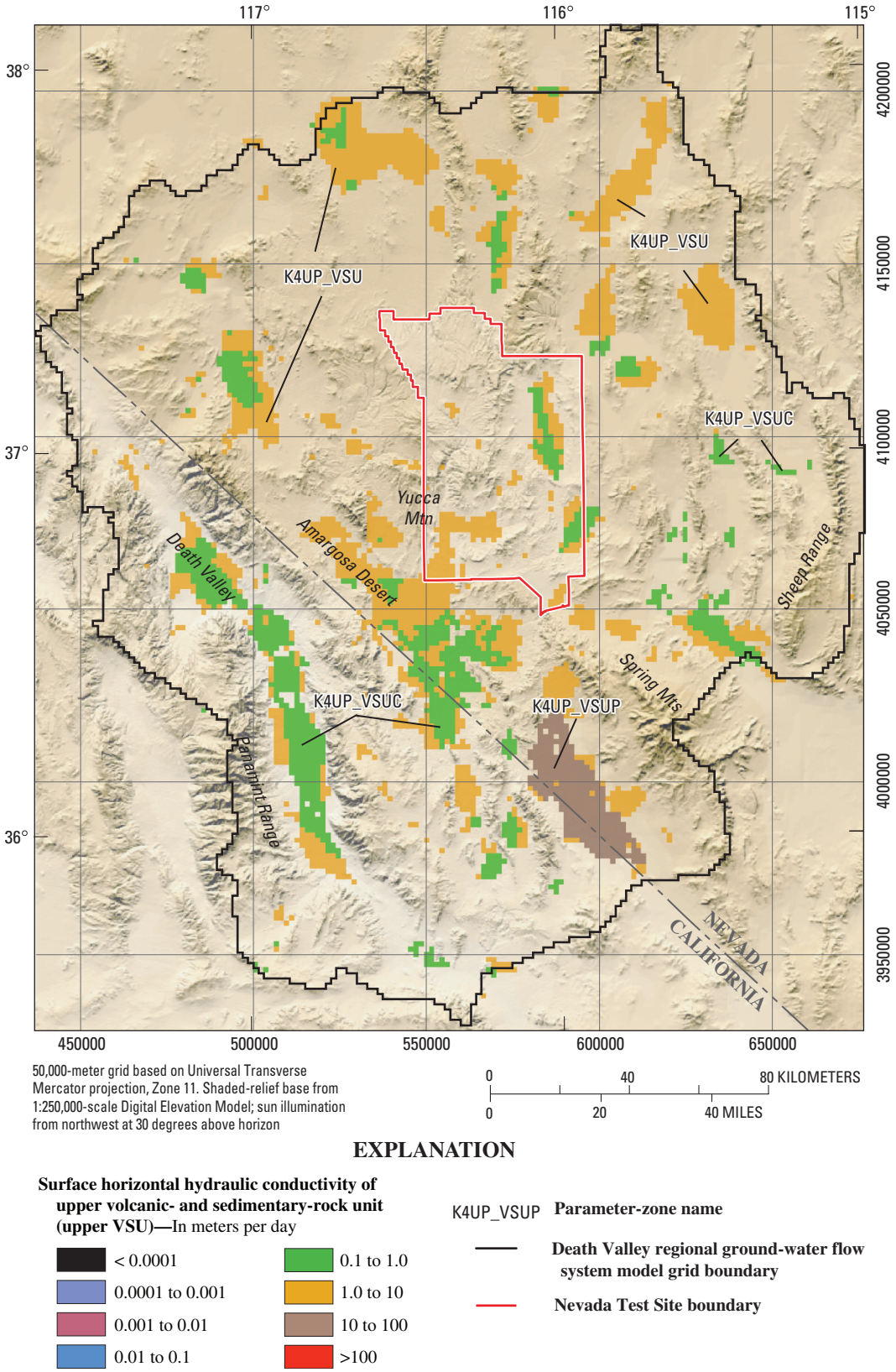

Figure F–30. Hydraulic-conductivity zone parameters, unit thickness, and extent for upper volcanic- and sedimentary-rock unit.

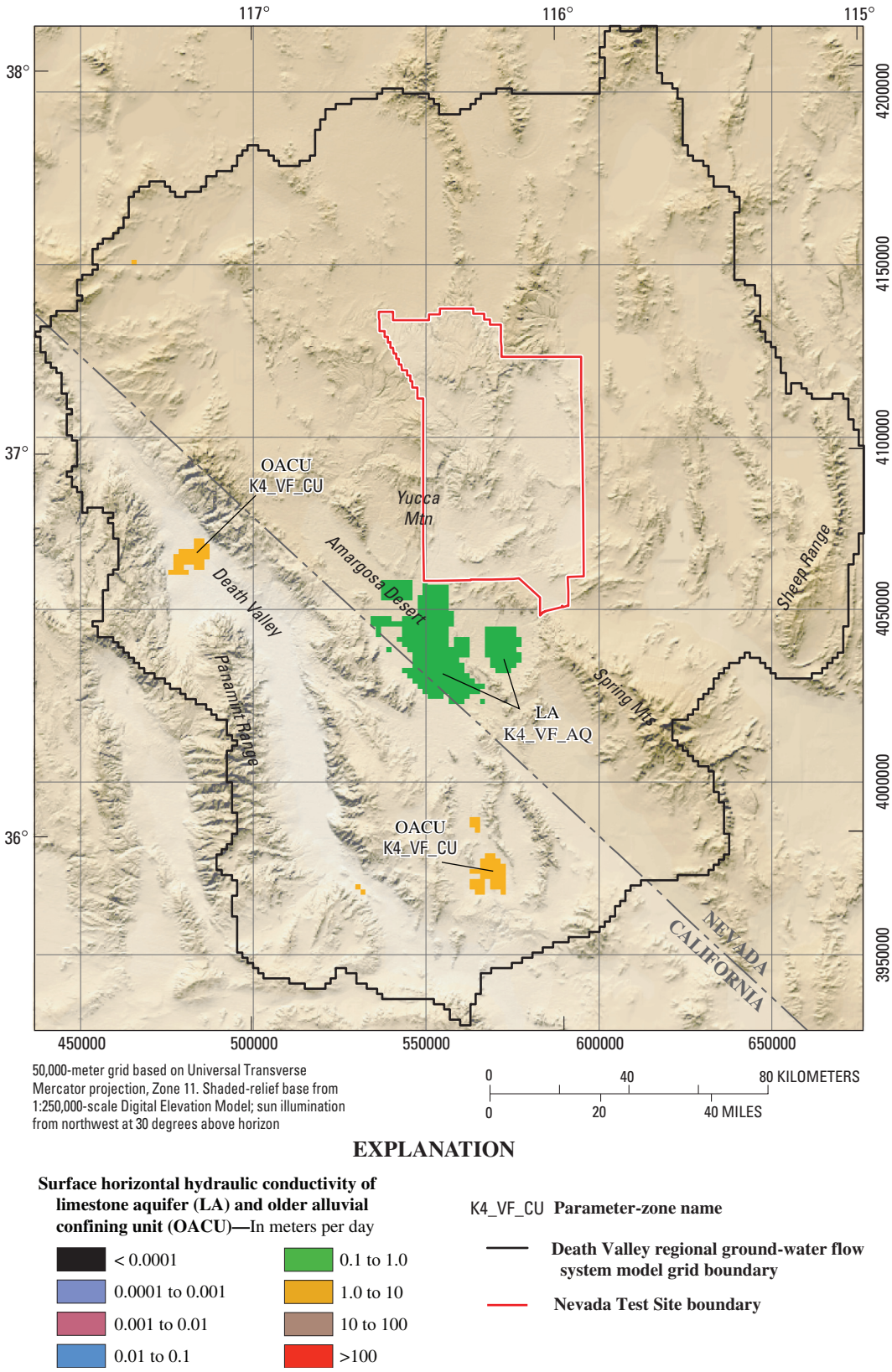

Figure F–31. Hydraulic-conductivity zone parameters, unit thickness, and extent for limestone aquifer and older alluvial confining units.

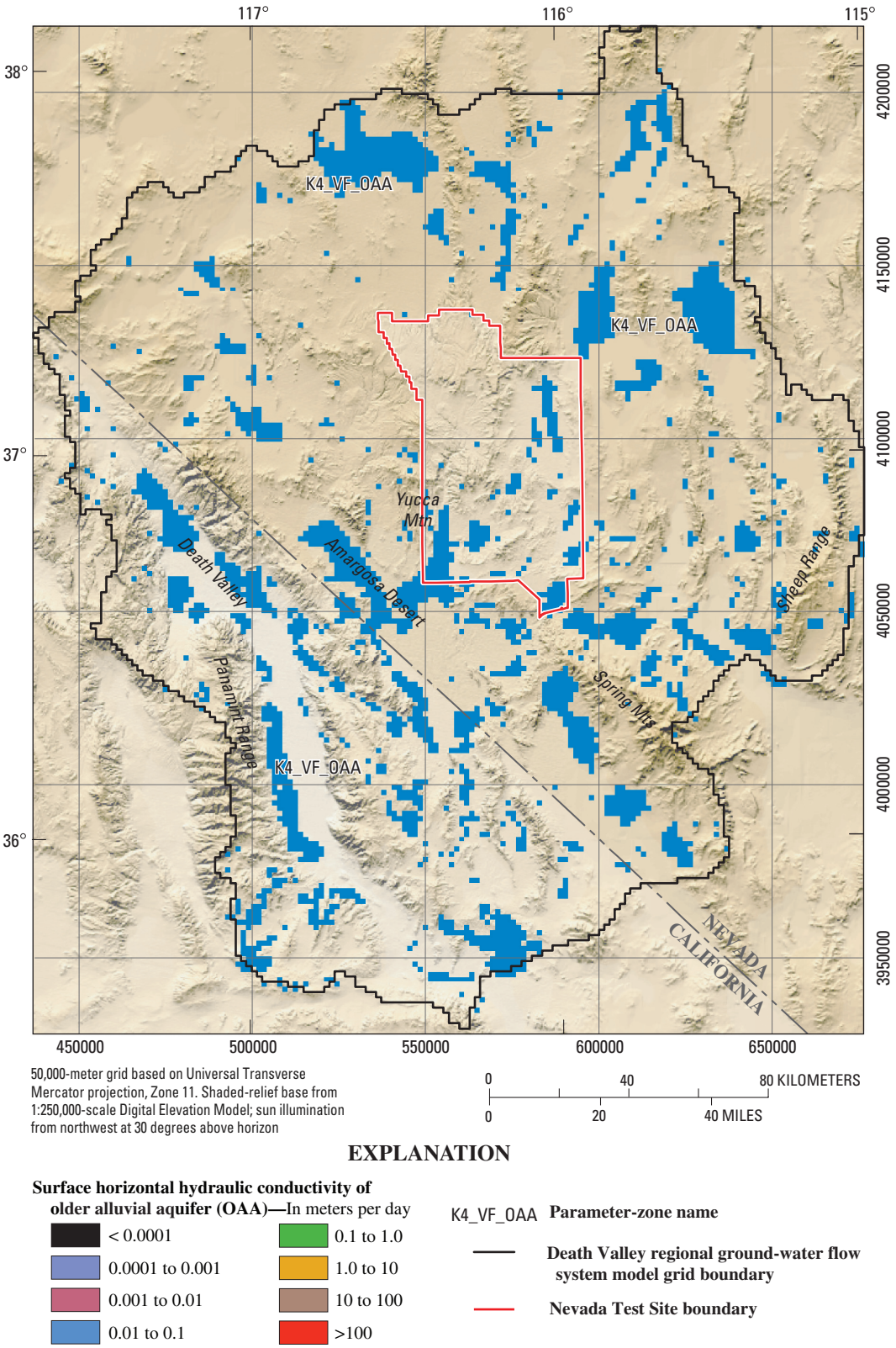

Figure F–32. Hydraulic-conductivity zone parameters, unit thickness, and extent for older alluvial aquifer.

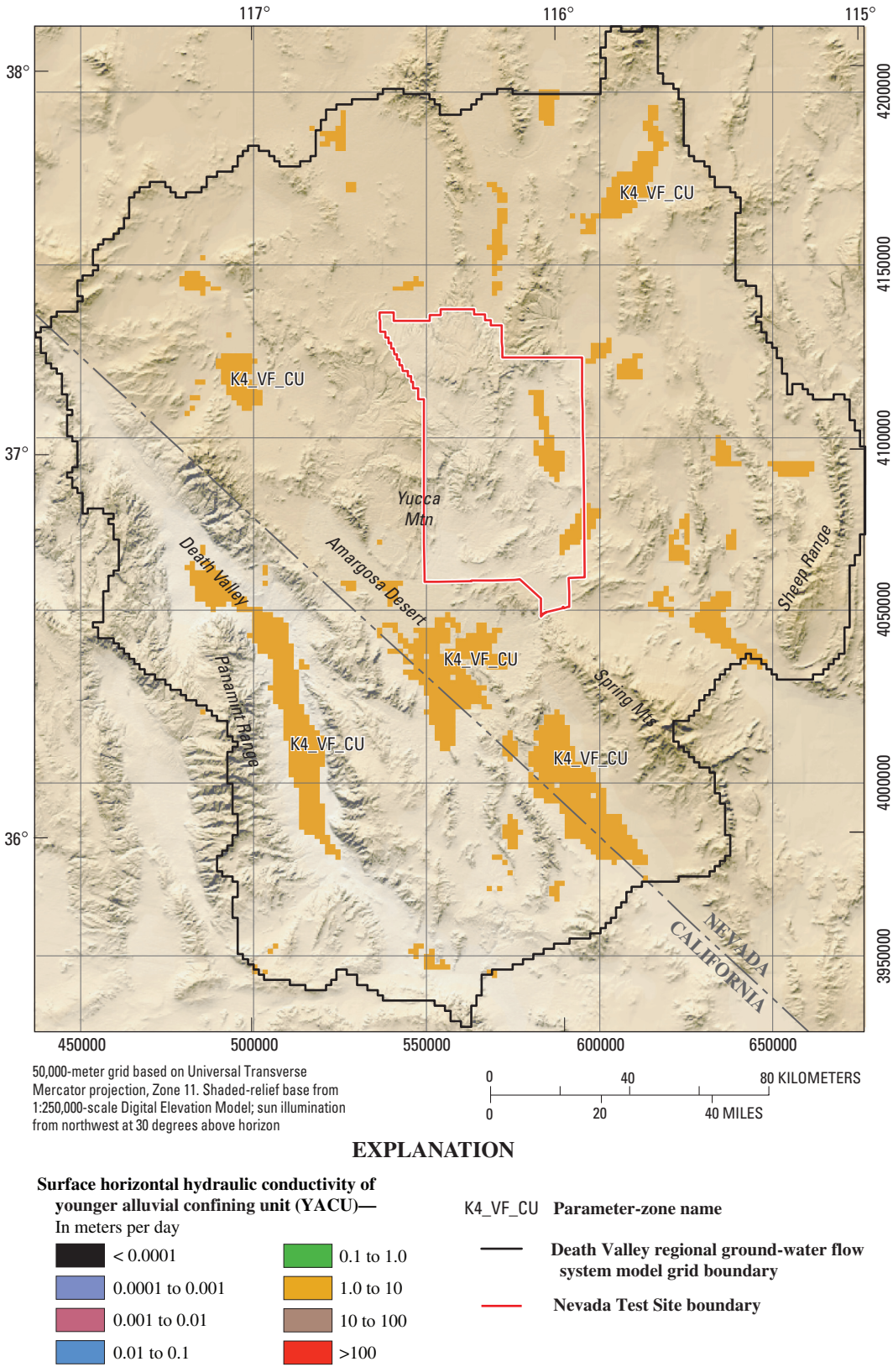

Figure F–33. Hydraulic-conductivity zone parameters, unit thickness, and extent for younger alluvial confining unit.

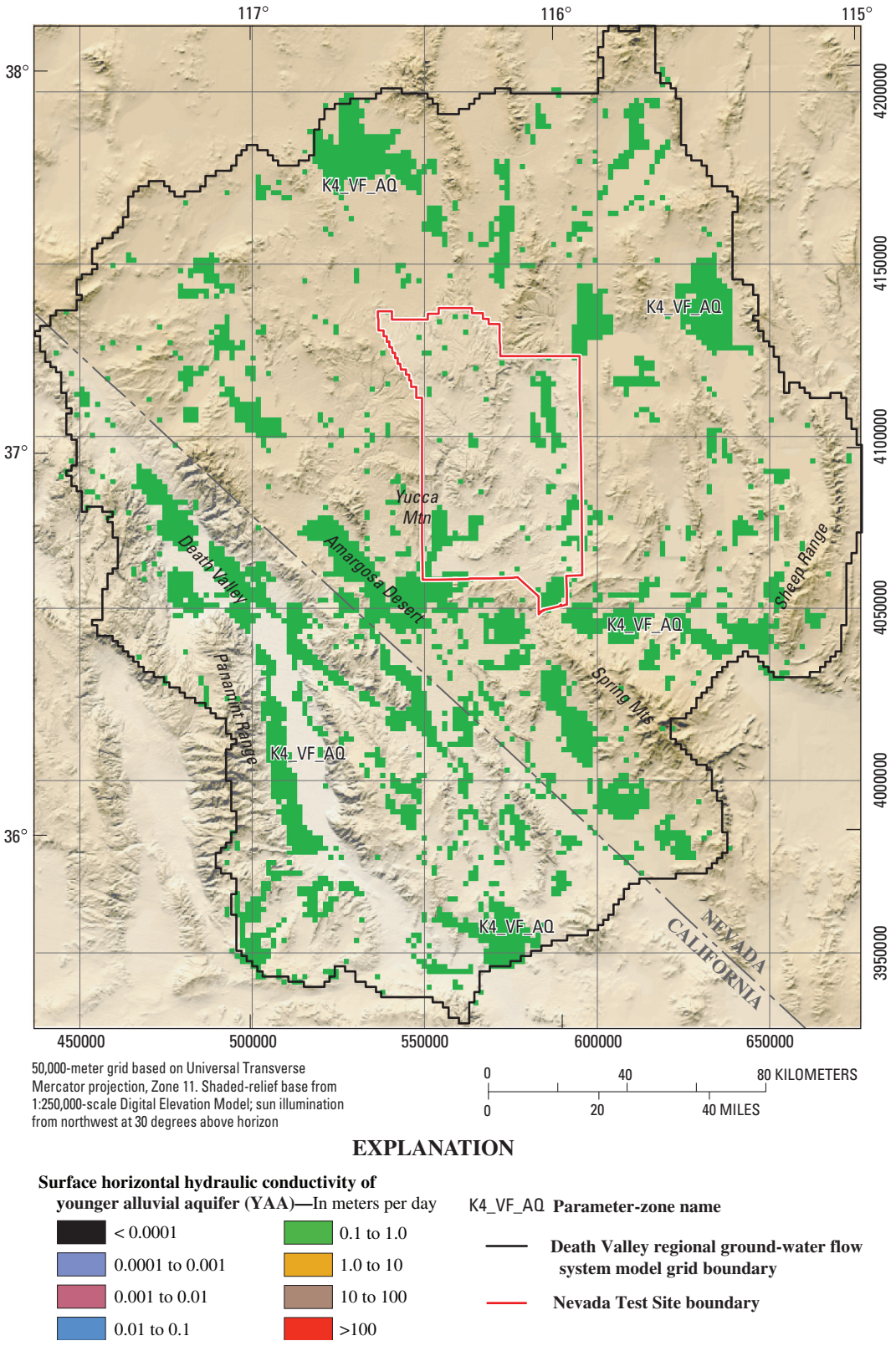

Figure F–34. Hydraulic-conductivity zone parameters, unit thickness, and extent for younger alluvial aquifer unit.

Table F–12. Calibrated depth-decay parameters.

[Abbreviations: LCA, lower carbonate-rock aquifer; LCCU, lower clastic-rock confining unit; NA, not applicable; TSDVS, Tertiary sediments, Death Valley section; UCA, upper carbonate-rock aquifer; UCCU, upper clastic-rock confining unit; VSU, volcanic- and sedimentary-rock unit; YAA, younger alluvial aquifer; YACU, younger alluvial confining unit]

Parameter name	Description	Initial depth-decay parameter value (IT Corp., 1996b)	Depth-decay parameter value (percentage of surface hydraulic conductivity at 1,000 meters)	Composite scaled sensitivity	Coefficient of variation[1]
KDEP_LCA	LCA (except as noted in KDP_LCANO, KDP_LCAT1 and KDEP_NO)	[2]0.00102	0.00010 (79.4%)	1.7	NA
KDP_LCANO	LCA (K243GV_LCA, K24ISM_LCA, K243PP_LCA, and K2_DV_LCA)	[2]0.00102	0.00002894 (93.6%)	0.4	NA
KDP_LCAT1	(1) LCA_T1 (2) LCA (K2421FLCA)	[2]0.00102	0.0015 (3.2%)	3.1	NA
KDP_VOL	Volcanic rocks	[3]0.00256	0.00248 (0.33%)	7.3	NA
KDEP_UCCU	UCCU and UCA	[4]0.0015	0.0015 (3.2%)	1.0	NA
KDEP_VFVL	Basin fill (YAA, YACU, OAA, OACU, and LA)	[5]0.00563	0.0123 (<0.005%)	0.2	0.5
KDEP_VSUU	Upper VSU	[6]0.004	0.0043457 (0.005%)	1.0	0.002
KDEP_VSUL	Lower VSU	[6]0.004	0.00012 (75.9%)	0.6	NA
KDEP_NO	(1) LCCU_T1 (2) LCCU (except as noted in KDEP_XL) (3) LCA (K2rr_LCA) (4) LFU (5) SCU (6) XCU (K11CXILCU) (7) ICU	[7]0.0012	0.0000001 (99.98%)	7.9×10^{-4}	NA
KDEP_XL	(1) XCU (2) LCCU (K1LCCU_XCU)	[8]0.0015	0.00061972 (24%)	1.7	NA

[1]Values were not log transformed.

[2]Mean exponential depth-decay coefficient for carbonate-rock aquifers.

[3]Mean exponential depth-decay coefficient for volcanic-rock aquifers.

[4]Exponential depth-decay coefficient for the UCCU.

[5]Mean exponential depth-decay coefficient for alluvial (basin-fill) aquifers.

[6]Exponential depth-decay coefficient for TSDVS.

[7]Exponential depth-decay coefficient for LCCU.

[8]Exponential depth-decay coefficient for intrusive rocks.

Vertical Anisotropy

Vertical anisotropy parameters were initially defined for the four major rock types and generally had small *CSS* values during steady-state simulations (table F–13). Pumping stresses the upper part of the system and tends to force water to flow more vertically than under a natural hydraulic gradient. This resulted in greater sensitivity to vertical anisotropy parameters during transient simulations. The basin-fill units, in which much of the pumpage occurs, were most sensitive (table F–13). These units also are most likely to have stratification that would tend to decrease the vertical conductivity relative to the horizontal (anisotropy ratios greater than 1).

Storage Properties

During calibration, conceptual models simulating the top of the DVRFS model as confined or unconfined model layers were evaluated. Confined conditions were simulated with the capability of the HUF package (Anderman and Hill, 2003). The unconfined simulations were numerically unstable and ultimately were abandoned. For most confined simulations (including the final calibration), the top of the model was defined using simulated hydraulic heads from the previous model run. Because the cones of depression caused by pumpage in this system are fairly modest, simulated results should be very close to results obtained with unconfined simulations.

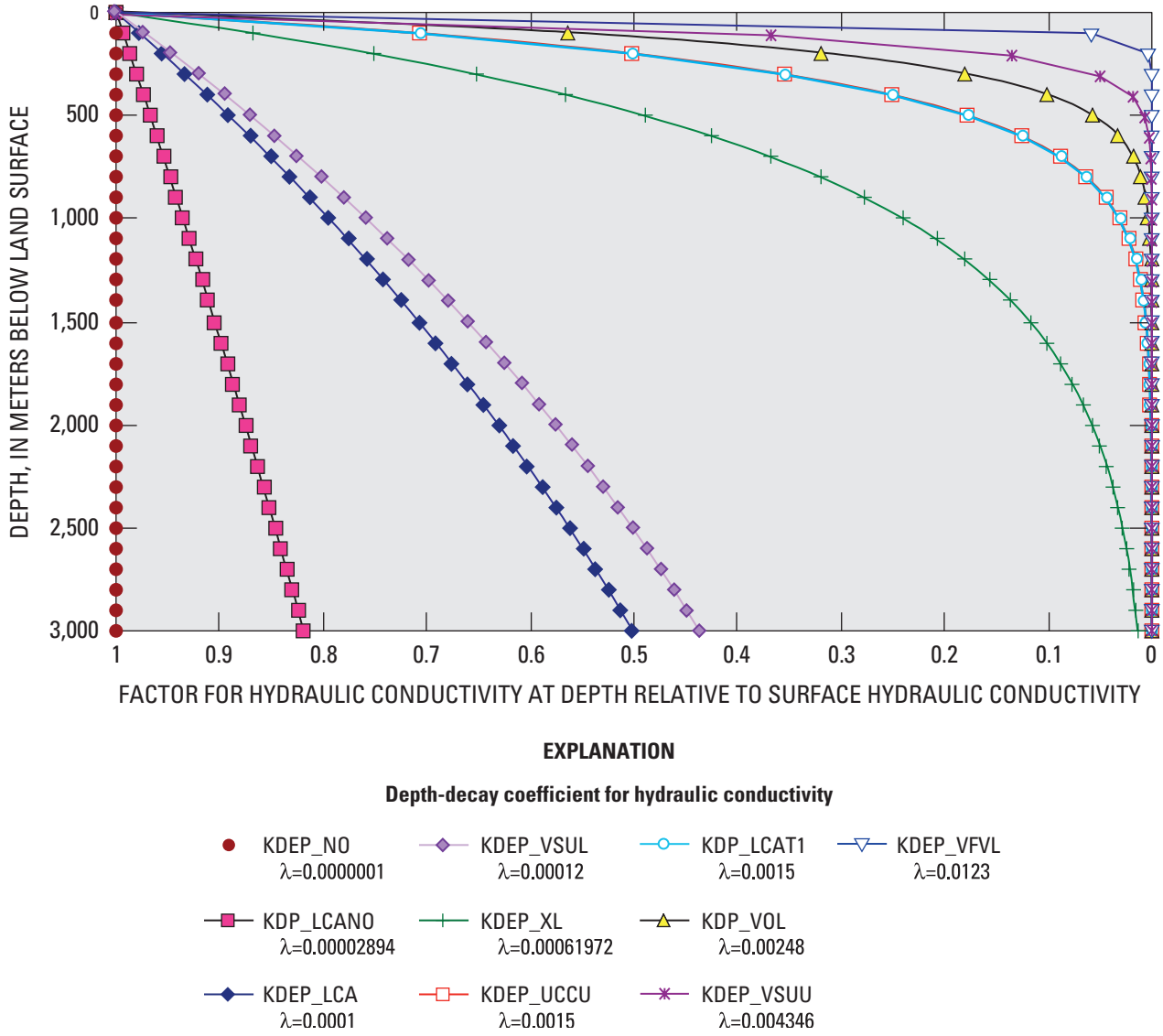

Figure F–35. Hydraulic conductivity values decreasing with depth relative to the surface hydraulic conductivity. The value of each depth-decay parameter is listed for each parameter.

Specific-storage values were determined from literature for the various HGUs in the model domain (table F–14). Specific-storage (Ss) values were used for model layers 2 through 16, and a specific yield (Sy) value was used for layer 1. Storativity values estimated from aquifer tests (Anderson and Woessner, 1992; Belcher and others, 2001) and other modeling studies in the region (Thomas and others, 1996; Schaeffer and Harrill, 1995) are similar to the values used in the DVRFS model (table F–14).

Specifying unique storage property values for each HGU was not necessary. Only those units strongly affected by pumping (predominantly the basin-fill units) were categorized by more than one storage property value. Parameter estimation methods did not provide reasonable storage property values; those values were always unreasonably high. As a result, values of specific storage and specific yield consistent with the literature (Thomas and others, 1989; Anderson and Woessner, 1992; Schaeffer and Harrill, 1995; Belcher and others, 2001) were specified (set by the user) and the hydraulic conductivities in the basin-fill units, which were most affected by pumping, were re-estimated. Model fit was much better with relatively high values of specific yield. Hence, these values were specified near the upper end of the reasonable range. Errors in simulated heads and discharges associated with errors in storage property values likely are small and were not quantified.

Hydrogeologic Structures

Many of the HFB parameters (fig. F–5) had little effect on the simulation of heads and discharges and were removed as barriers from the flow model. In the final calibration, only nine barriers had a significant effect on heads and discharges

Table F–13. Calibrated vertical anisotropy parameters.

[Abbreviations: ICU, intrusive-rock confining unit; LCA, lower carbonate-rock aquifer; LCA_T1, thrusted lower carbonate-rock aquifer; LCCU, lower clastic-rock confining unit; LCCU_T1, thrusted lower clastic-rock confining unit; NA, not applicable; OAA, older alluvial aquifer; OACU, older alluvial confining unit; UCCU, upper clastic-rock confining unit; XCU, crystalline-rock confining unit; YAA, younger alluvial aquifer; YACU, younger alluvial confining unit]

Parameter name	Description	Vertical anisotropy value[1]	Composite scaled sensitivity	Coefficient of variation[2]
K1_VANI	Confining units (XCU, ICU, UCCU, LCCU, and LCCU_T1)	1.267	0.132	0.5
K2CARBVANI	UCA, LCA, and LCA_T1	1.00	0.125	0.5
K3_VOLVANI	Volcanic-rock units	1.00	0.273	0.47
K4_VFVANIA	Basin-fill aquifers (YAA, OAA, coarser grained parts of upper VSU)	5,000.0	0.119	NA
K4_VFVANIC	Basin-fill confining units (YACU, OACU, finer grained parts of upper VSU)	5,000.0	0.215	NA
K4_VFVANVL	Lower VSU	2.184	0.233	0.5

[1]Ratio of horizontal to vertical (values less than 1 indicate higher vertical than horizontal hydraulic conductivity).

[2]Values were log transformed.

Table F–14. Calibrated storage property values.

[Specific-yield values were used for layer 1, specific-storage values were used for layers 2–16. Values in parentheses for comparison with storage-property values. Abbreviations: ICU, intrusive-rock confining unit; LCCU, lower clastic-rock confining unit; LCCU_T1, thrusted lower clastic-rock confining unit; OAA, older alluvial aquifer; OACU, older alluvial confining unit; UCCU, upper clastic-rock confining unit; XCU, crystalline-rock confining unit; YAA, younger alluvial aquifer; YACU, younger alluvial confining unit]

Parameter name	Description	Range of storage properties (specific storage m^{-1})	Composite scaled sensitivity	Storage parameter value
STOR_12	Confining units (XCU, ICU, UCCU, LCCU, LCCU_T1); Carbonate-rock aquifers (LCA, LCA_T1, UCA)	[1]1.5×10^{-8} – [2]6.3×10^{-2}	16,127.0	7.0×10^{-8}
STOR_34	Volcanic-rock units; Lower VSU; Basin-fill aquifers (YAA, OAA, LA, upper VSU)	[3]9.7×10^{-7} – [4]2×10^{-2}	5,598.5	1.0×10^{-5}
STOR_4VUP	Upper VSU - fine grained, Pahrump Valley	[3]4.7×10^{-7} – [2]4×10^{-2}	424.9	7.5×10^{-5}
STOR_4C	Basin-fill confining units (YACU, OACU)	[3]4.7×10^{-7} – [2]4×10^{-2}	50.6	5.0×10^{-5}
SY_OTHER	Specific yield for layer 1 in basin-fill units outside the Pahrump Valley (except for upper and lower VSU)	[1,2,3,4]0.001 – 0.47	9.5	1.9×10^{-1}
SY_PAH	Specific yield for layer 1 in basin-fill units in the Pahrump Valley	[1,2,3,4]0.001 – 0.47	13.1	2.0×10^{-1}
SY_PUMP	Specific yield for layer 1 in VSU (upper and lower) outside the Pahrump Valley	[1,2,3,4]0.001 – 0.47	8.7	1.9×10^{-1}

[1]Schaeffer and Harrill, 1995.

[2]Belcher and others, 2001.

[3]Thomas and others, 1996.

[4]Anderson and Woessner, 1992.

in that they supported the hydraulic gradients (table F–15 and fig. F–5). In particular, the B_LVVSZ_IS parameter (representing part of the LVVSZ) and the B_SOLTARIO parameter (representing the Solitario Canyon fault) have been well documented as to their potential effect on heads in the model domain and had a significant effect on the simulated heads. In most cases, the other potential barriers were found to be unimportant or were adequately represented by the juxtaposition of HGUs in the HFM (Chapter E, this volume).

Recharge

Recharge in the DVRFS model was initially defined using one parameter to vary the net infiltration (Hevesi and others, 2003) throughout the entire model domain by a constant factor (fig. F–6). The *CSS* value for this parameter during initial model runs was high and generally within the top three most sensitive parameters, indicating that adequate observations existed to describe recharge with additional parameters. Early model runs tended to overestimate net recharge, as was

Table F–15. Calibrated hydraulic characteristic parameters for hydrogeologic structures defined as horizontal-flow barriers.

[Abbreviations: NA, not applicable]

Parameter name	Description	Hydraulic characteristic parameter value (meters per day per meter)	Composite scaled sensitivity	Coefficient of variation[1]
B_HWY95	Highway 95 fault	2.95×10^{-4}	0.046	0.09
B_DVFC_FCR	Death Valley fault zone–Furnace Creek fault zone	1.00×10^{-7}	0.008	0.03
B_LVVSZ_1	Las Vegas Valley shear zone	9.00×10^{-4}	0.005	NA
B_LVVSZ_I2	Las Vegas Valley shear zone	4.19×10^{-8}	0.135	NA
B_PAHRUMP	Pahrump Valley part of Pahrump-Stewart Valley fault zone	5.52×10^{-7}	0.267	0.5
B_LVVSZ_IS	Unnamed splay of the Las Vegas Valley shear zone near Indian Springs	1.1×10^{-8}	0.046	NA
B_DV_N	Northern Death Valley-Furnace Creek fault	2.40×10^{-7}	0.247	NA
B_SOLTARIO	Solitario Canyon fault	4.45×10^{-5}	0.214	NA
B_TC_LINE	Thirsty Canyon lineament	1.00×10^{-7}	0.008	NA

[1]Values were log transformed.

evident from comparing the infiltration rates to the ET and spring-flow discharge observations. A recharge zone multiplication array adjusted the net infiltration model (Hevesi and others, 2003) to fit the discharge observations.

The net-infiltration distribution accounted only for surficial characteristics of the system and not the hydraulic conductivity of the rocks at the water table (Hevesi and others, 2003). Thus, in some areas large recharge rates into rocks with low hydraulic conductivity produced unrealistic simulated hydraulic heads. In reality, the recharge likely was redistributed in the process of percolation. To account for this dynamic, the distribution of recharge was modified by essentially moving high recharge rates from areas where the rocks at the water table were relatively low in permeability to downgradient areas where the rocks at the water table were relatively permeable. This was done by combining net-infiltration rates and the relative permeability of the rocks in the upper five model layers to produce the zones of recharge distribution (fig. F–36). The resulting recharge parameters were multipliers for net infiltration (table F–16).

The parameter zones were created by classifying the top five model layers as either consisting of predominantly (more than 50 percent) relatively higher permeability aquifer material (basin-fill, volcanic-rock, and carbonate-rock aquifers) or relatively lower permeability rocks not identified as aquifers. Cells with aquifer material represent areas where greater permeability would allow rapid infiltration. Because cells with aquifer materials receive most of the infiltration, these cells were further defined by rock type. The logarithm of the infiltration rate was classified into five zones representing areas with no infiltration to those with high infiltration rates. These two classifications (permeabiltiy based on rock type and infiltration rates) were combined into the parameters described in table F–16. Some of the parameters were insensitive, so they were combined with parameters having similar recharge multiplier values.

Separate parameters defined for recharge on the high-altitude, carbonate-rock aquifer material contributed the largest volumes of water to the ground-water system (parameters RCH_2 and RCH_8). High recharge rates on the Spring Mountains were necessary to properly simulate discharge in Pahrump Valley, Shoshone and Tecopa basins, Amargosa Desert, and Indian Springs (figs. F–6 and F–36). Parameter RCH_2 was used for recharge on the carbonate-rock aquifer, generally in the Spring Mountains and southern part of the Sheep Range (simulated mean recharge of about 70 millimeters per year [mm/yr]). Parameter RCH_8 was used in the eastern and central western (simulated mean recharge of about 38 mm/yr) part of the model domain. In the final calibration, recharge on the Spring Mountains was 76 percent of the value of net infiltration, whereas recharge on the northeastern and central western parts of the model domain was about 100 percent of the estimate of net infiltration (table F–16). The magnitude of the reduction of net infiltration seems reasonable considering that the composition of the carbonate-rock aquifer material is quite variable between these two areas of the model domain, and the extremely high estimate of net infiltration in the Spring Mountains could not be supported by rocks in the area.

During calibration, a ninth recharge zone was added (RCH_9) where infiltration rates exceeded the hydraulic-conductivity value of the underlying rocks and water ponded more than 20 m above land surface. The recharge rate was assumed to be negligible in these areas, and the recharge parameters (multipliers) in adjacent zones were increased.

In general, the estimated recharge was distributed similarly to the net-infiltration rate of Hevesi and others (2003). For the entire model domain, 92 percent of the net infiltration estimated by Hevesi and others (2003) or 303,415 cubic meters per day was simulated as recharge.

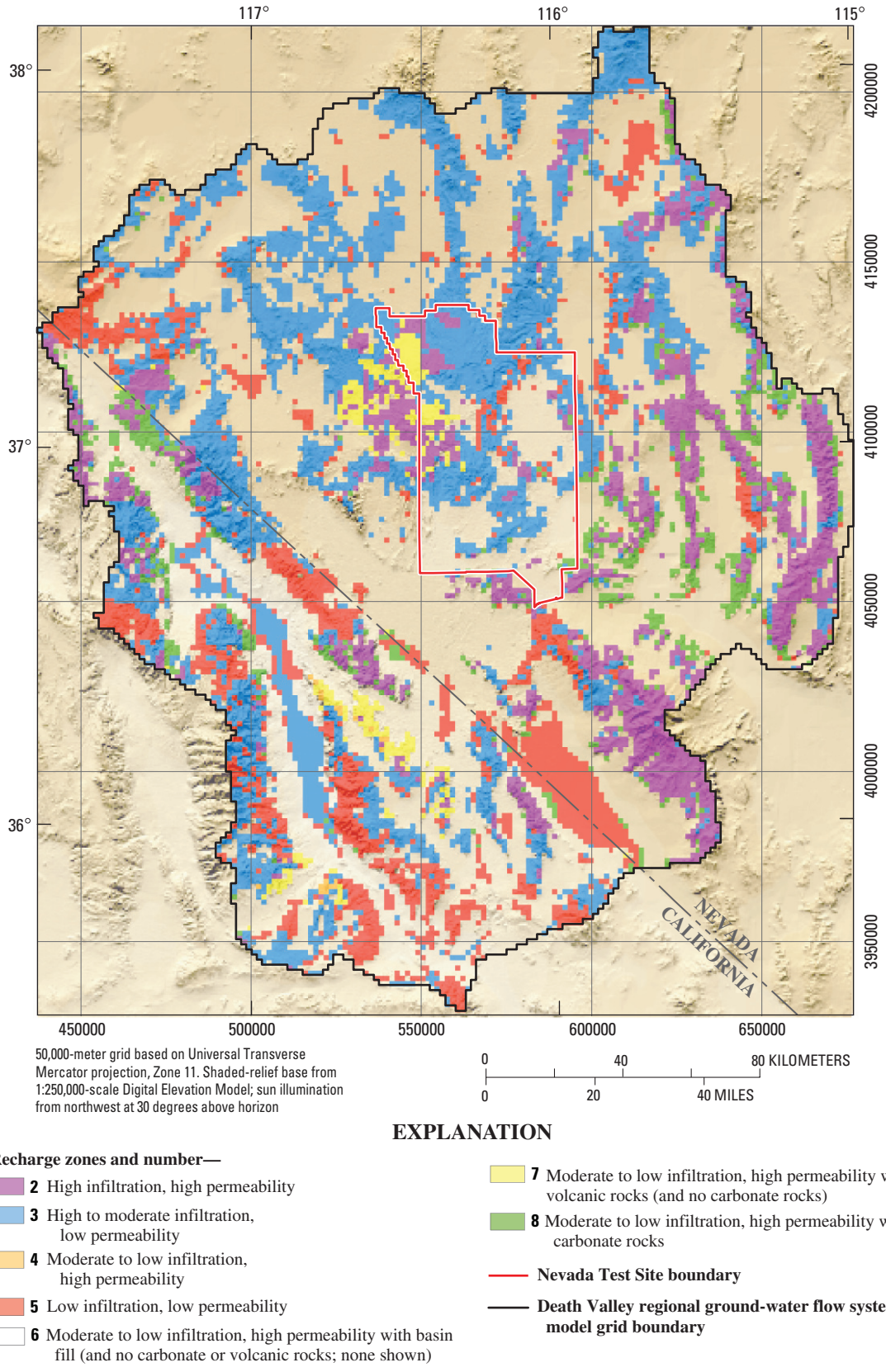

Figure F–36. Recharge zone multiplication array representing infiltration rates and relative permeability in upper five model layers.

Table F–16. Calibrated recharge parameters used as multipliers for infiltration rates defined for the recharge zones.

[NA, not applicable]

Recharge zone number	Relative permeability	Relative infiltration rate	Description	Recharge parameter name	Recharge parameter value[1]	Composite-scaled sensitivity	Coefficient of variation[2]
1	NA	None	No infiltration	NA	NA	NA	NA
2	High	High	High infiltration and high permeability (generally carbonate rocks in the Spring Mountains and southern part of the Sheep Range)	RCH_2	0.76	3.22	0.10
3	Low	High to moderate	High to moderate infiltration and low permeability (generally volcanic and(or) clastic rocks)	RCH_35	1.12	3.46	0.13
5	Low	Low	Low infiltration and low permeability (generally volcanic and(or) clastic rocks)	RCH_35	1.12	3.46	0.13
4	High	Moderate to low	Moderate to low infiltration and high permeability on various rock types	RCH_467	1.00	0.115	0.5
6	High	Moderate to low	Moderate to low infiltration and high permeability with basin-fill aquifers present in the upper five layers	RCH_467	1.00	0.115	0.5
7	High	Moderate to low	Moderate to low infiltration and high permeability with volcanic rocks present in the upper five layers	RCH_467	1.00	0.115	0.5
8	High	Moderate to low	Moderate to low infiltration and high permeability with carbonate rocks present in the upper five layers (eastern and central western part of the model domain)	RCH_8	1.00	0.0648	0.5
9	NA	NA	Cells where recharge exceeded hydraulic conductivity	RCH_9	0.000001	0.28×10^{-8}	NA

[1]The net-infiltration array values (fig. C–8) are multiplied by this value to calculate the simulated recharge (fig. F–6).

[2]Values were log transformed.

Ground-Water Discharge

The discharges through ET and spring flow were treated as observations in the flow model, and the conductances of the drain cells were estimated. Initially, the drain cells were divided into five types with the following parameter names (table F–17): (1) DEEP_DRN, warm-water discharge indicates rapid flow from depth and the drain cell is located at the shallowest occurrence of the LCA; (2) UPPER_DRN, flow is through surficial materials that are coarser than playa materials (YAA and OAA); (3) UP_PLY_DRN, flow is through surficial fine-grained playa materials (YACU and OACU); (4) UP_DV_DRN, springs in Death Valley that have substantial salt concentrations; and (5) UP_PAH_DRN, all discharge areas in Pahrump Valley where estimates of discharge over time are available. During calibration, drain conductance parameters were added for the northern part of Death Valley (UP_DVN_DRN) and the Furnace Creek area (FRNCR_DRN).

Hydraulic-Head and Discharge Observations

During calibration, 4,899 observations of hydraulic head and 49 of ground-water discharge and their corresponding weights were evaluated to assess whether the weighting scheme appropriately contributed to model fit. During calibration, weights on five hydraulic-head observations were decreased because of high sensitivity values. Weights on head-change observations in these same locations with particularly large weights also were decreased.

During calibration, the effect of data clustering was examined. The possibility that clustering contributed to the poor fit in areas where observations were limited was tested by grossly increasing the weights on some of the sparsely distributed observations during selected model runs. Because increased weights never significantly improved model fit at these data-sparse locations, calibration difficulties were attributed to some aspect of the model framework or hydrologic conceptualization. The problem then was investigated by examining the hydrologic conceptualization, indicating that

Table F–17. Calibrated drain conductance parameters.

[m/d/m, meter per day per meter; NA, not applicable]

Parameter	Description	Composite scaled sensitivity	Parameter value[1] (m/d/m)	Coefficient of variation[2]
DEEP_DRN	Deep, warm-water springs	1.86	45.6	0.50
UPPER_DRN	Springs in coarse-grained basin-fill deposits	0.70	107.8	0.50
UP_PLY_DRN	Springs in playa deposits	1.78	83.9	0.50
UP_DV_DRN	Death Valley springs with high salt concentrations	0.00855	10,000.0	NA
UP_PAH_DRN	Springs in Pahrump Valley	1.66	195.3	0.50
UP_DVN_DRN	Springs in the northern part of Death Valley	0.145	52.8	0.50
FRNCR_DRN	Spring in the Furnace Creek area	0.00149	10,000.0	NA

[1]The parameter value equals the conductance at most cells.

[2]Values were not log transformed.

data clustering is not a significant problem because most of the data clusters are in areas of high hydraulic conductivity, where the sensitivity of hydraulic heads to most parameters is relatively small.

Ground-water discharge observations did not vary throughout the steady-state or transient stress periods, except for Manse and Bennetts Springs in Pahrump Valley. For these springs, one steady-state and two transient discharge observations from 1960 and 1998 were used. All other ground-water discharge observations only appear once in the objective function (eq. 8a). The 49 ground-water discharge observations were combined into 45 discharge observation locations by combining the three observations for Manse and Bennetts Springs into one observation location for each spring.

Modifications also were made to ground-water-discharge observation CVs during the calibration process (but not the observations themselves) because the determination of CVs may not have considered adequately all sources of observation error. Model error, discharge-estimation methods, and magnitude of discharge rate were considered during the calibration process and, where necessary, CVs were modified to reflect (1) the cumulative error, (2) the relative observation importance, and (3) the confidence in the observation.

Final Calibration of Model

As described above, numerous conceptual models were evaluated to test the validity of interpretations of the flow system. For each conceptual model, a new set of parameters was estimated and the resulting simulated hydraulic heads, drawdowns, and ground-water discharges were compared to the observations. Only those conceptual model changes contributing to a significant improvement in model fit were retained. Figures F–37 and F–38 present the estimated parameter values for the final calibration. Figure F–37 shows the values for the hydraulic-conductivity parameters for the confining units, the carbonate-rock units, the volcanic units, and the basin-fill units. Figure F–38 shows the values for the conductances for the drain parameters, the net-infiltration multiplication factor for the recharge parameters, the values for specific storage and specific yields for the storage property parameters, the values for the vertical anisotropy parameters, and the hydraulic characteristics for the HFB parameters.

Model Evaluation

The calibrated DVRFS model was evaluated to assess the likely accuracy of simulated results. An advantage of using nonlinear regression to calibrate the model is that a substantial methodology exists for model evaluation that facilitates a better understanding of model strengths and weaknesses. A protocol exists to evaluate the likely accuracy of simulated hydraulic heads and ground-water discharges, estimated and specified parameter values and associated sensitivities and confidence intervals, and other measures of parameter and prediction uncertainty. As part of the model evaluation, the regional water budget, the model fit, values of parameter estimates and their associated sensitivities, and boundary flows were evaluated. A qualitative analysis also was performed by comparing the hydrologic conceptual model (Chapter D, this volume) to the overall simulation in several hydrologically significant areas.

Regional Water Budget

The simulated water budgets for the DVRFS for the steady-state prepumping stress period and transient stress period 86 are presented in table F–18 and figure F–39. Stress period 86 (representing year 1997) was used to evaluate the model because there were many observations, and all components except storage were quantified. Many of the observations were quantified with significant accuracy, and some were used as observations in model calibration. The greatest uncertainty is in the representation of recharge.

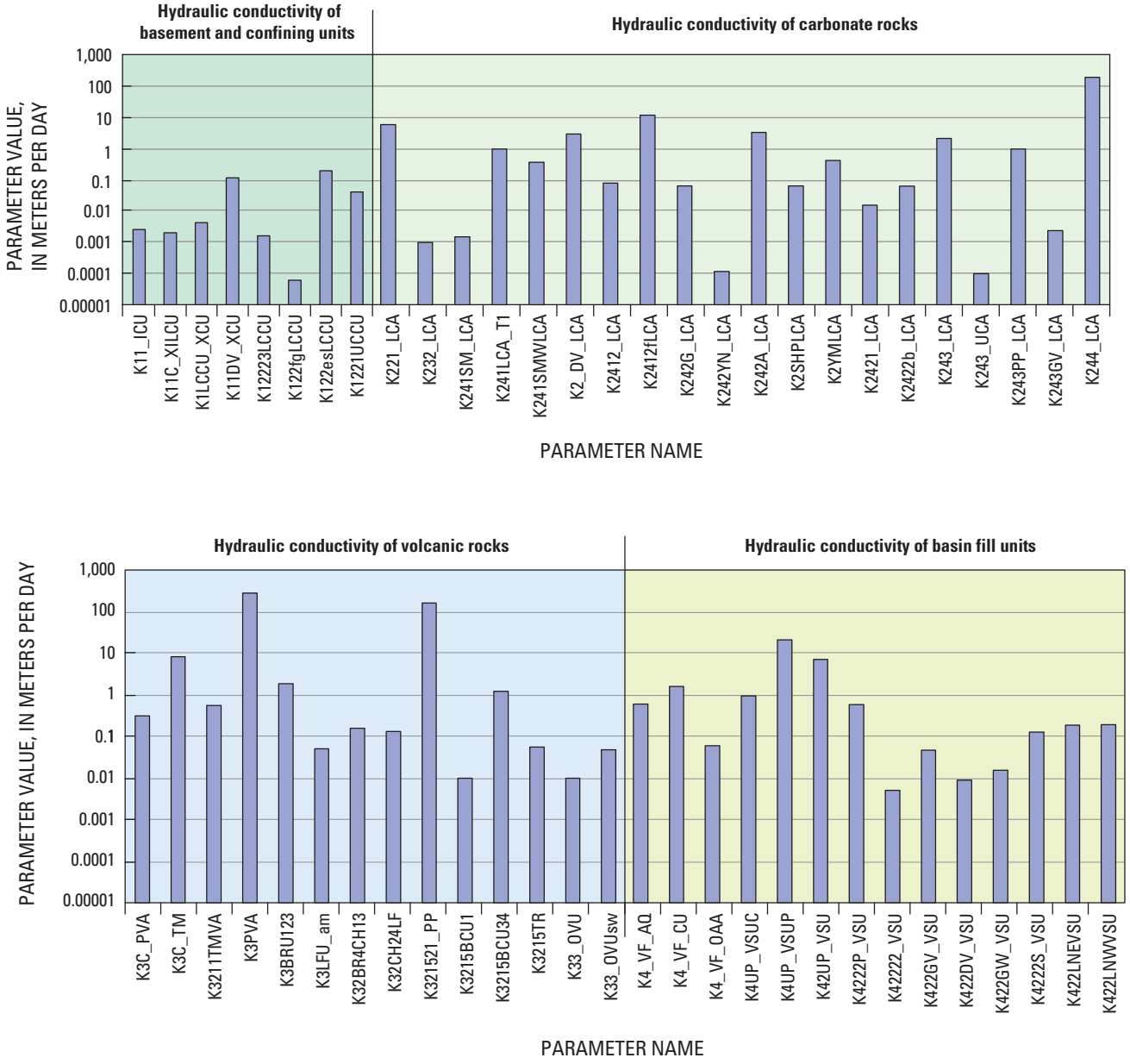

Figure F–37. Parameter values defining hydraulic conductivity for confining units and carbonate rocks, volcanic rocks, and basin-fill units.

Simulated discharges decrease slightly from 361,523 m^3/d for the prepumping steady-state stress period to 344,870 m^3/d in 1998 (figs. F–39 and F–40). This change can be attributed mostly to pumpage in Pahrump Valley (fig. F–9 and table F–4). In 1997 (transient stress period 86), the sum of observed ground-water discharge is 313,203 m^3/d; and the sum of all simulated ground-water discharge is 344,870 m^3/d. As of 1998, most of the pumpage came from aquifer storage and is only just beginning to affect the regional discharge from ET and spring flow (fig. F–39).

Flow paths were simulated to evaluate flow directions in the model. For the most part, the model simulates the conceptual model described in Chapter D (this volume). The major exception was that discharge at the Furnace Creek Wash springs (fig. A–1 in Chapter A, this volume) appears to originate from beneath the north-northwestern part of the Amargosa Desert and areas within the SWNVF rather than from the Spring Mountains through Ash Meadows.

Evaluation of Model Fit to Observations

Model fit is initially evaluated using summary statistics (table F–19) and then through more detailed evaluations, including (1) consideration of results from the prepumping steady-state stress period and the final transient stress period,

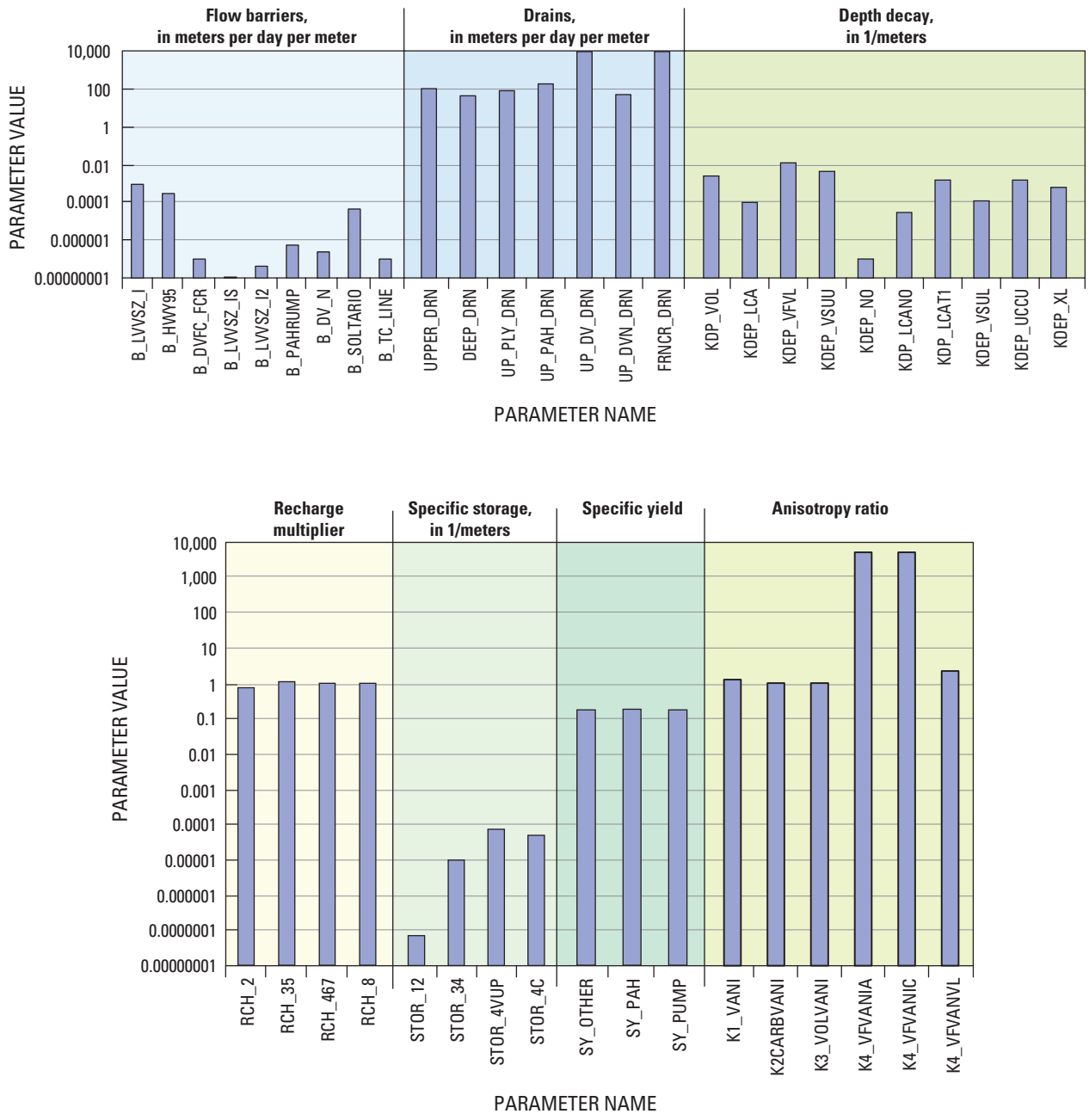

Figure F–38. Parameter values defining flow barriers, drains, and depth decay, recharge, storage, specific yield, and ratio of horizontal to vertical anisotropy.

(2) inspection of hydrographs calculated during transient stress periods, (3) assessment of spatial and temporal distribution of weighted and unweighted residuals, and (4) several graphical analyses. The sum of squared weighted residuals (SOSWR) are shown for completeness but indicate little about model fit. However, the square root of SOSWR divided by the number of observations (Nobs) provides a measure of model fit relative to the weighting that can be compared for different types of observations. A value of 1.0 indicates a match that is, overall, consistent with the observation error evaluation used to determine the weighting. The largest value, 5.4, is for constant-head boundary flow observations, indicating that the boundary flows are more poorly fit relative to the expected fit than are other types of observations. The second largest value, 3.6, was calculated for discharge observations. The CVs for discharges range from 10 to 71 percent (table F–4). Thus, on average, the difference between observed and simulated discharge can range from 36 to 360 percent of the observed discharge. Although the match to discharges is generally good and considered acceptable (fig. F–41), head-change data fit the observations best, relative to the standard deviations used to weight them.

Table F–18. Simulated and observed water budget for the steady-state prepumping stress period and transient stress period 86 (year 1997).

[ET, evapotranspiration; --, not available for combined observations; NA, not applicable]

Water-budget component	Steady-state prepumping stress period				Transient stress period 86, year 1997			
	Observed[1] (cubic meters per day)	Simulated[1] (cubic meters per day)	Fractional difference[2]	Coefficient of variation	Observed[1] (cubic meters per day)	Simulated[1] (cubic meters per day)	Fractional difference[2]	Coefficient of variation
Northern Death Valley Subregion								
FLOW IN								
Constant-head segment:								
Clayton	667	7,150	–9.72	0.75	667	7,240	–9.85	0.75
Eureka–Saline	15,100	15,700	–0.04	0.5	15,100	15,906	–0.05	0.5
Stone Cabin–Railroad	12,476	81,500	–5.53	0.96	12,476	85,305	–5.84	0.96
Panamint	15,000	25,400	–0.69	0.5	15,000	25,985	–0.73	0.5
FLOW OUT								
Discharge:[6]								
Sarcobatus Flat ET	–44,662	–27,458	0.39	--	–44,662	–39,340	0.12	--
Grapevine Canyon Springs	–3,485	–3,245	0.07	--	–3,485	–3,247	0.07	--
Central Death Valley Subregion								
FLOW IN								
Constant-head segment:								
Garden–Coal	[6]2,334	12,700	–4.44	0.86	[6]2,334	12,678	–4.43	0.86
FLOW OUT								
Constant-head segment:								
Las Vegas	[6]–3,633	–1,400	0.61	0.96	[6]–3,633	–1,396	0.62	0.96
Sheep Range	–18,747	–47,390	–1.53	--	–18,747	–47,324	–1.52	--
Pahranagat	[6]–3,040	–38,210	–11.57	--	[6]–3,040	–38,548	–11.68	--
Discharge:[6]								
Penoyer Valley ET	–12,833	–8,040	0.37	0.5	–12,833	–4,890	0.62	0.5
Oasis Valley ET	–20,311	–23,810	–0.17	--	–20,311	–23,630	–0.16	--
Indian Springs area	–2,240	–798	0.64	0.10	–2,240	0	1.00	0.10
Ash Meadows ET	–60,372	–64,106	0.06	--	–60,372	–61,098	–0.01	--
Franklin Well area ET	–1,150	–638	0.45	0.5	–1,150	–520	0.55	0.5
Franklin Lake ET	–3,519	–7,690	–1.19	--	–3,519	–7,240	1.06	--
Death Valley area springs and ET	–128,334	–186,020	–0.45	--	–128,334	–190,690	–0.49	--
Southern Death Valley Subregion								
FLOW IN								
Constant-head segment:								
Silurian	[6]500	–1,550	4.10	1.00	[6]500	3,710	4.12	1.00
Owlshead	[6]1,682	3,670	–1.18	0.89	[6]1,680	–1,560	–1.21	0.89
FLOW OUT								
Discharge:[6]								
Stewart Valley area ET	–3,379	–4,195	–0.24	--	–3,379	–3,842	0.14	--
Pahrump Valley area ET and springs	–32,400	–22,510	0.31	--	–3,378	–9,020	–1.67	--
Tecopa Basin area ET	–21,063	–3,806	0.82	--	–21,063	–3,807	0.82	--
Shoshone Valley area ET	–7,015	–3,620	0.48	--	–7,015	–3,650	0.48	--
Chicago Valley area ET	–1,462	–5,440	–2.72	0.36	–1,462	–5,420	–2.71	0.36

Table F–18. Simulated and observed water budget for the steady-state prepumping stress period and transient stress period 86 (year 1997).—Continued

[ET, evapotranspiration; --, not available for combined observations; NA, not applicable]

Water-budget component	Steady-state prepumping stress period				Transient stress period 86, year 1997			
	Observed[1] (cubic meters per day)	Simulated[1] (cubic meters per day)	Fractional difference[2]	Coefficient of variation	Observed[1] (cubic meters per day)	Simulated[1] (cubic meters per day)	Fractional difference[2]	Coefficient of variation
Southern Death Valley Subregion—Continued								
Total IN, constant heads	[6]47,759	144,570 (339,601)	--	--	[6]47,759	[7]149,264 (341,275)	--	--
Pumpage[3]	0	0	0	--	--	46,150	--	--
Storage	0	0	0	--	--	221,266	--	--
Recharge	[4]<342,000	303,415	NA	--	--	303,415	--	--
TOTAL IN:	<397,513	[7]447,985 (643,017)	--	--		[7]723,615 (720,095)		
Total OUT, constant heads	[6]–25,420	[7]–87,000 (281,913)	--	--	[6]–25,420	[7]–87,000 (–282,306)	--	--
Total, discharge:	–342,225	–361,523	–0.06	--	–313,203	–344,870	–0.07	--
Pumpage	0	0	0	--	NA	–275,978	NA	--
Storage	0	0	0	--	NA	–9,147	NA	--
TOTAL OUT:	--	–448,523 (–342,250)	--	--	NA	–912,301 (–912,302)	NA	--
FLOW IN – FLOW OUT:	--	[6,7]–538 (–420)	--	--	NA	[5,7]–192,206 (–194)	--	--

[1]Negative values indicate flow out of the model domain.

[2]Calculated as (observed–simulated)/observed.

[3] Simulated inflows are mostly from irrigation return flows and injection. A minor part of this is from well-bore inflow between pumping nodes connecting model layers in the Multi-Node Well package (Halford and Hanson, 2002).

[4]Total net infiltration from Hevesi and others (2003). Not used as an observation.

[5]The global budget error from the model in parenthesis. Steady-state is –0.07 percent, transient is –0.02 percent.

[6]Observed constant-head flow is less than that reported in table D–4 (this volume) because of no-flow boundaries applied in the model to subsegments where flow is less than 1,000 cubic meters per day.

[7]Value in parenthesis is cumulative numbers and takes into account flow in and out of given constant head segments. Individual constant head fluxes are composite numbers.

[8]Portions of Death Valley discharge are in northern and southern Death Valley subregion.

The standard error of regression (eq. 9) provides an overall measure of model fit. For the steady-state and transient simulations the standard error of the regression equals 2.7 (table F–19), which indicates that overall model fit is 2.7 times worse than would be consistent with the observation error statistics used to determine observation weights.

Ground-Water Discharge and Boundary Flow

Matching natural ground-water discharge from ET and springs was generally more difficult than matching hydraulic heads and hydraulic-head changes (table F–4) but provided important information for calibration. The overall fit of simulated ground-water discharge and boundary flow to observations is unbiased; simulated values plotted against observations are randomly scattered about the 1 to 1 line (fig. F–42*A*). Flow associated with the Stone Cabin–Railroad boundary segment (fig. A2–3 in Appendix 2, this volume) is an outlier where simulated flow into the model is higher than the observed flow. Most water entering the model along this northern boundary segment discharges at Sarcobatus Flat, where simulated discharge rates are less than the observed value. Fractional differences show how close the match was; the CV reflects expected observation error. If the model fits the observations in a manner that on average is as expected, the fractional differences would, on average, be similar to the CVs (table F–4). For the constant-head boundary flows, one weighted residual is greater than, and one weighted residual is less than, three times the standard error. Eighty-seven percent of the constant head boundary flows are within three times the standard error of regression.

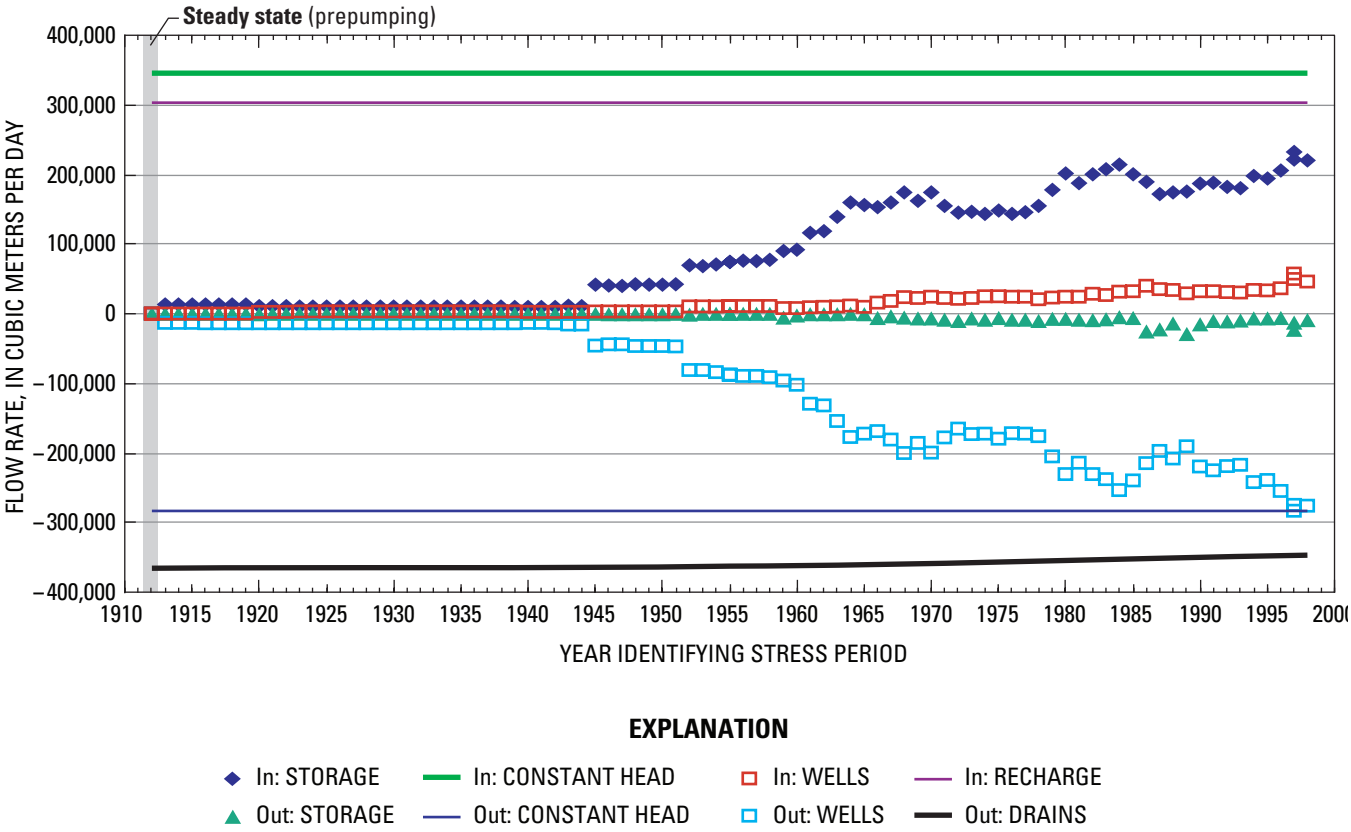

Figure F–39. Total simulated and observed ground-water discharge from evapotranspiration and spring flow for steady state and transient stress periods of the transient model.

Noting that ground-water discharges have been assigned a negative sign indicating flow out of the model, the weighted residuals for ground-water discharges appear to vary randomly about a value of zero with a slight overall bias toward being positive, indicating that simulated discharges in these areas are greater than observed discharges (fig. F–43). The greatest positive unweighted ground-water discharge residuals (simulated greater than observed) by volume (absolute value greater than 10,000 cubic meters/day) are at Death Valley (Cottonball Basin, middle, and Mesquite Flat) (OBS-DV-COTTN, OBS-DV-MIDDL, and OBS-DV-MESQU). The greatest negative unweighted ground-water discharge residuals (simulated less than observed) are at Sarcobatus-northeastern (OBS-SARCO-NE), early observations at Manse Spring in Pahrump (OBS-PAH-MANS) and upper Tecopa Valley (OBS-TC-TECOP). The two major discharge areas that contribute the largest error to the model are Death Valley and the Shoshone/Tecopa area. Two of the weighted residuals for ground-water discharges are greater than 8.2 and one is less than –8.2, indicating that 94 percent of the flow-weighted residuals are within three times the standard error of the regression. For the constant-head boundary flows, one weighted residual is greater than, and one weighted residual is less than three times the standard error. Eighty-seven percent of the constant head boundary flows are within three times the regression standard error.

The graph of weighted residuals for ground-water discharge (fig. F–43) indicates how well the model reproduces the observed discharges. An absolute value of 1.0 or less indicates that the residual was less than the standard deviation of the observation error. Weighted residuals that exceed 3.0 are considered to be large. For 35 of the 49 discharge observations, simulated ground-water discharge values are less than three times the standard error (fig. F–44). Simulated discharge from the regional ground-water discharge areas is shown in figure F–45. For these major discharge areas, simulated discharges are within one standard deviation, except at the Shoshone/Tecopa area and Death Valley.

Hydraulic Heads

Comparison of prepumping, steady-state simulated hydraulic heads (figs. F–46 and F–47) with the potentiometric surface of D'Agnese and others (1998) and the potentiometric surface of Appendix 1 (this volume) indicates that the DVRFS model results adequately depict major features of the hydraulic-head distribution. Local mounds of perched water (D'Agnese and others, 1998) are not represented in this simulation. In general, areas of nearly flat and steep hydraulic gradients are appropriately located and important hydraulic gradients are represented:

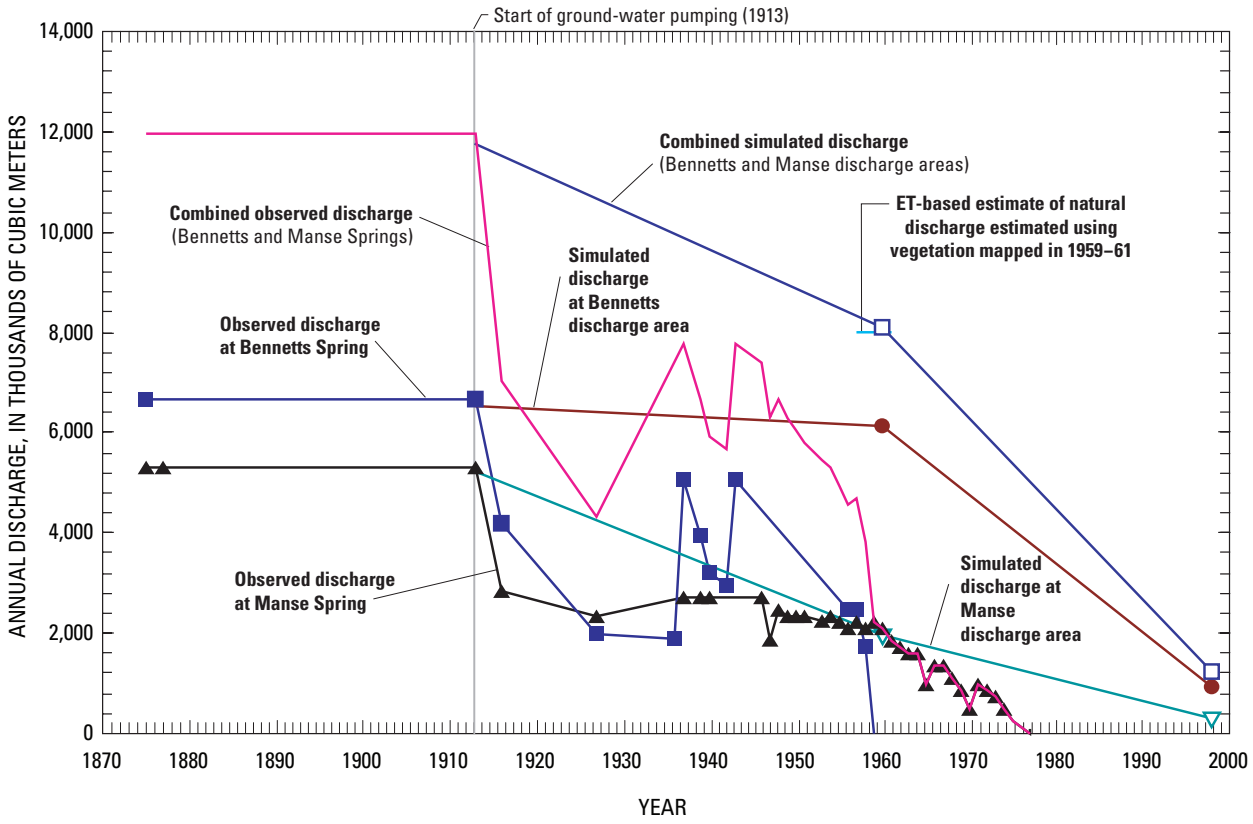

Figure F–40. Simulated and observed annual discharge from regional springs in Pahrump Valley.

Table F–19. Summary statistics for measure of model fit.

[SOSWR, sum of squared weighted residuals; Nobs, number of observations]

Type of observation	Number of observations	Average positive weighted residual	Average negative weighted residual	SOSWR	[SOSWR/Nobs]$^{1/2}$
Hydraulic head	2,227	2.1	–1.8	22,702	3.2
Hydraulic-head changes—transient[1]	2,672	1.6	–1.4	13,361	2.2
Discharge	49	2.9	–2.3	637	3.6
Constant-head boundary flow	15	3.7	–3.3	438	5.4
Total	**4,963**	**1.8**	**–1.6**	**37,146**	**2.7**
Other statistics					
Number of defined parameters	100				
Number of estimated parameters	Variable				
Standard error of the regression	2.7				

[1]Steady-state head observations are included with transient head observations if they are (1) classified as steady-state conditions and (2) located where there were no head observations during the initial steady-state stress period.

(1) The potentiometric-surface trough on Pahute Mesa, although subdued in the simulation, is represented;

(2) The generally west-to-east hydraulic gradient in the volcanic rocks at Yucca Mountain is simulated;

(3) The upward vertical hydraulic gradients from the carbonate-rock aquifer at Yucca Mountain are represented in the simulation (pl. 2, hydrograph [HG] 26); and

(4) The downward vertical hydraulic gradients in recharge areas of the Spring Mountains (pl. 2) and parts of Pahute Mesa (pl. 2, HG 18. 20, and 28) and upward vertical hydraulic gradients in discharge areas in Pahrump Valley (pl. 2, HGs 11, 12, and 14) and Ash Meadows (pl. 2, HG 1) are represented.

Simulated values plotted against observations generally fall on the 1 to 1 line, indicating a good model fit (fig. F–42*B*). The fit of simulated to observed hydraulic heads is generally

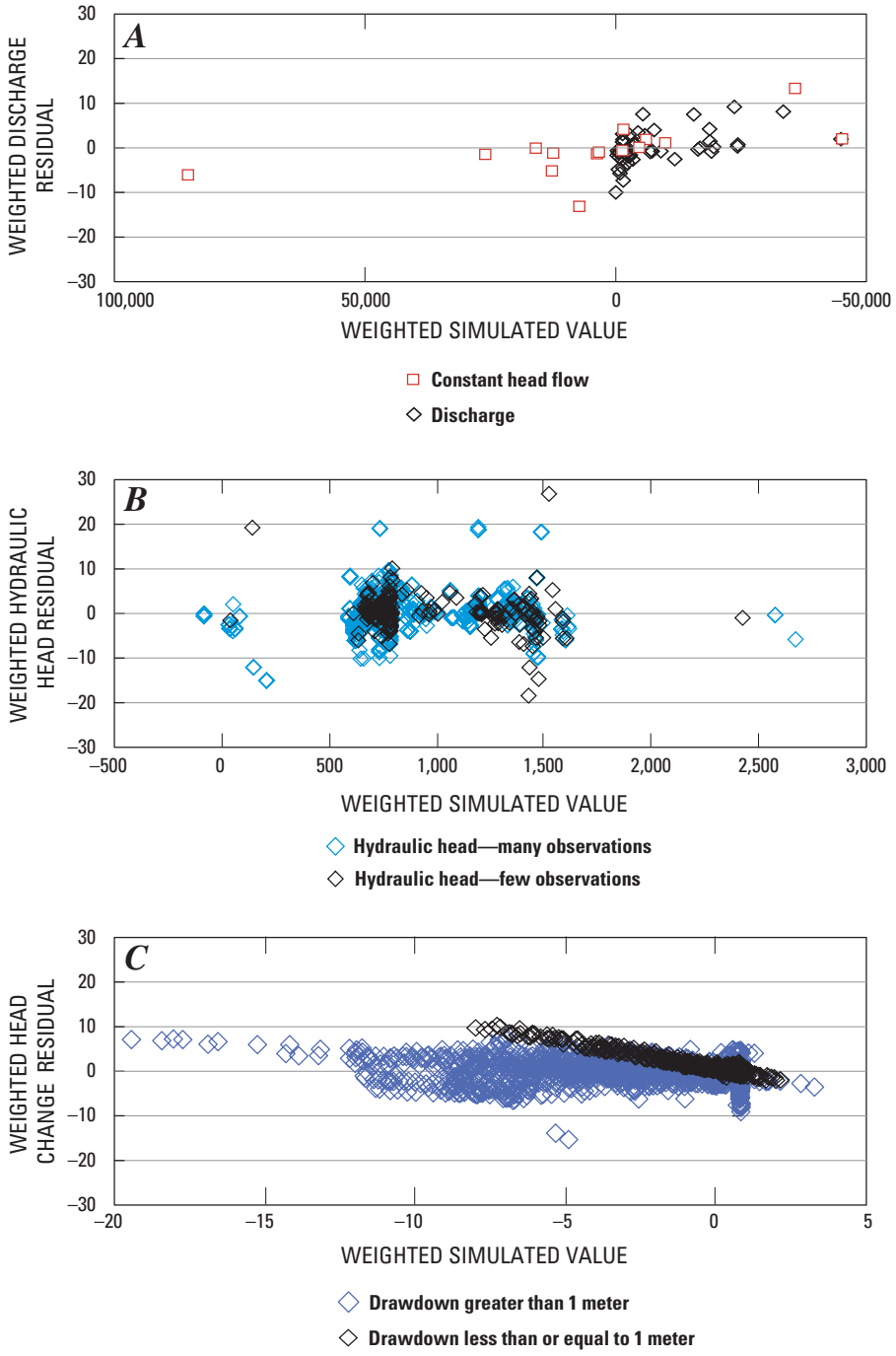

Figure F–41. Weighted residuals and simulated equivalent for (*A*) hydraulic head, (*B*) head change, and (*C*) constant-head flow and discharge.

good (unweighted residuals with absolute values less than 10 m) in most areas of nearly flat hydraulic gradients and moderate (residuals with absolute values of 10 to 20 m) in the remainder of the nearly flat hydraulic gradient areas (primarily in Pahrump Valley) (fig. F–46). The fit of simulated to observed heads is poorer (residuals with absolute values of greater than 20 m) in areas of steep hydraulic gradient. Poorest fit to observed hydraulic heads is in the vicinity of the steep hydraulic gradient along the Eleana Range and western part of Yucca Flat, and in the southern part of the Owlshead Mountains (fig. F–46). The fits also are poor in the southern part of the Bullfrog Hills and the north-northwestern part of the model domain. Most of these larger residuals can be attributed to (1) insufficient representation of the hydrogeology in the HFM, (2) misinterpretation of water levels, (3) model error associated with grid cell size, or (4) a combination of the first three factors.

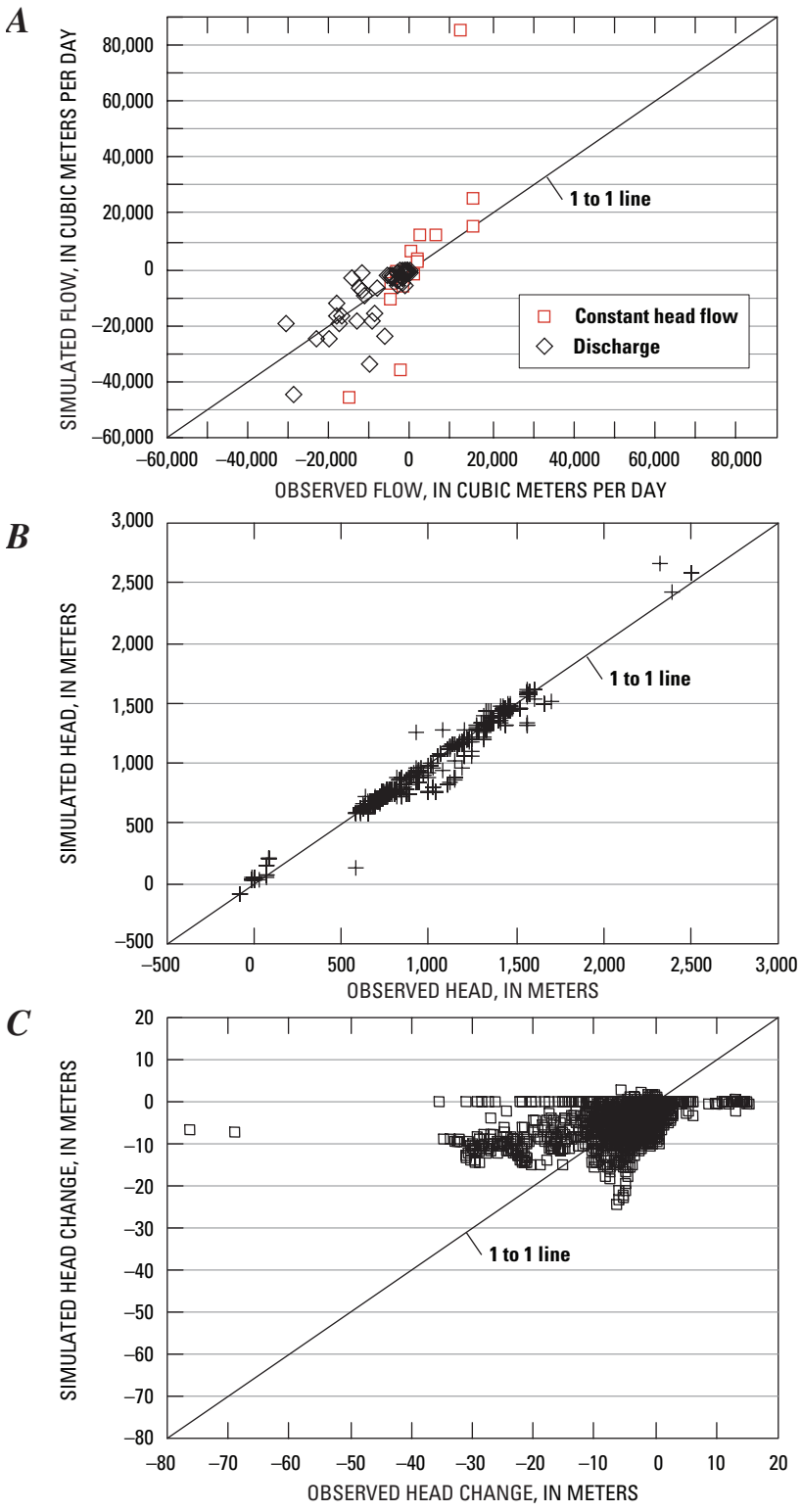

Figure F–42. Weighted observed value compared to weighted simulated values for (*A*) hydraulic head, (*B*) head change, and (*C*) constant-head flow and discharge.

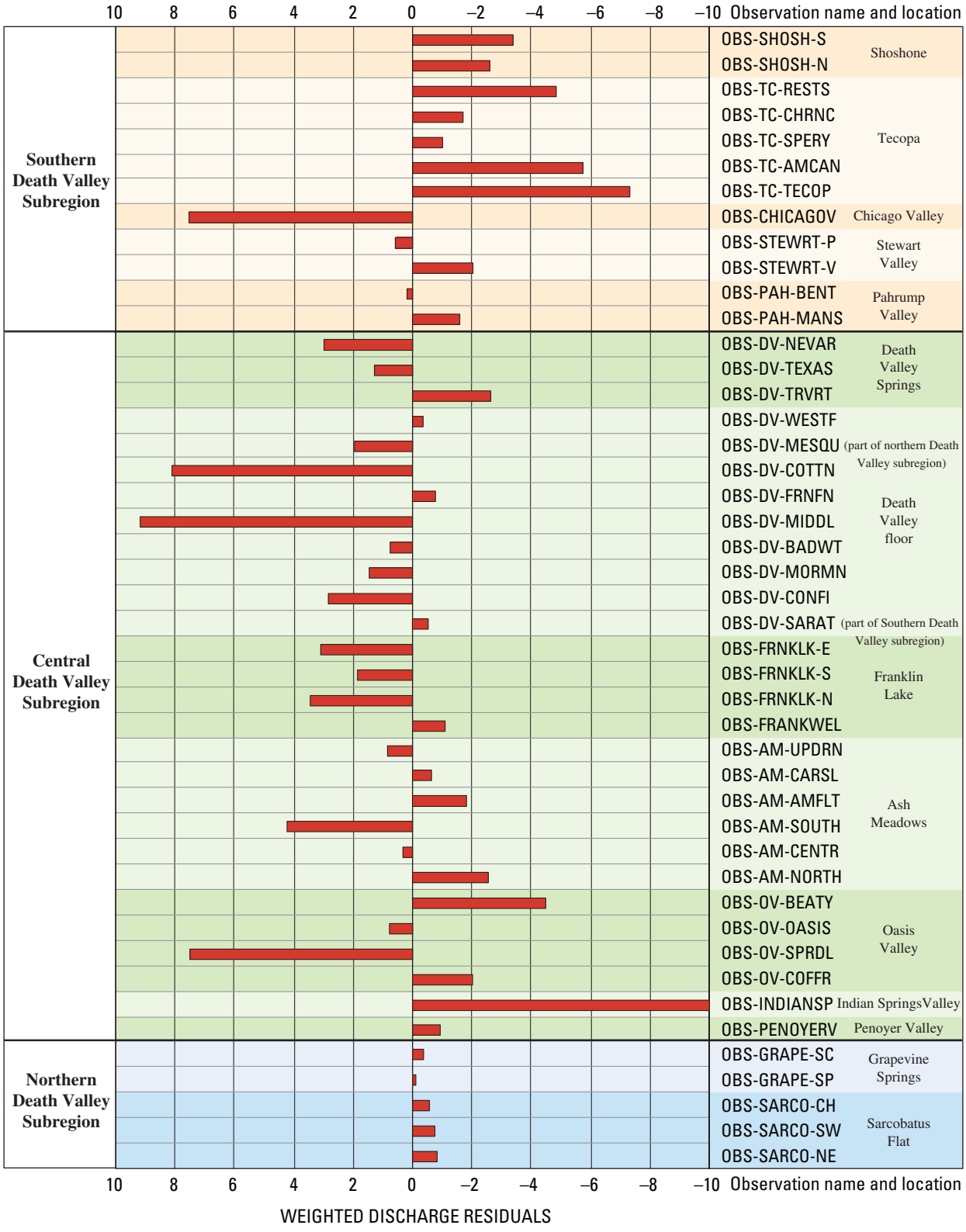

Figure F–43. Ground-water discharge weighted residuals (observed minus simulated).

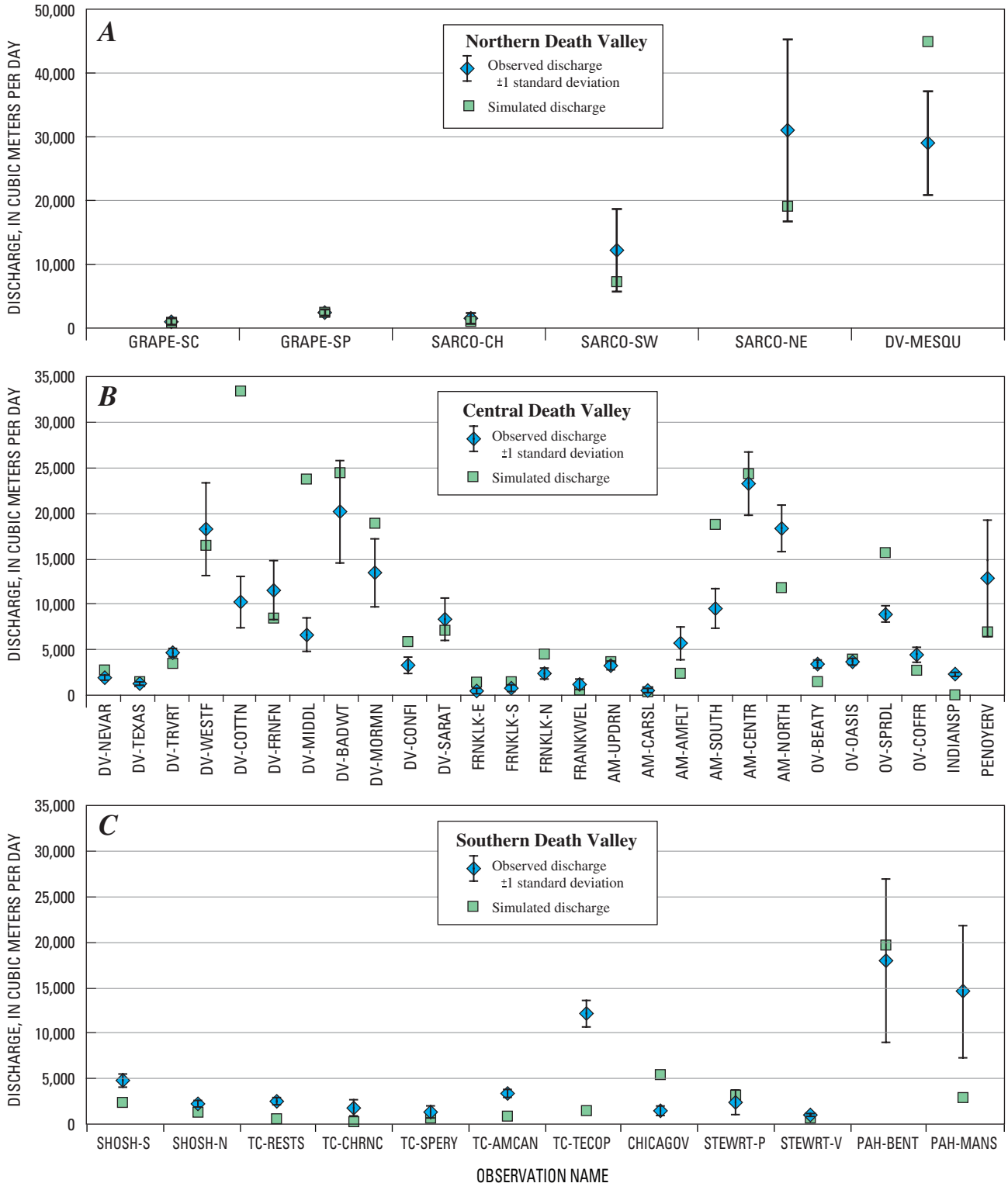

Figure F–44. Observed and simulated ground-water discharge by subregion: (*A*) Northern Death Valley, (*B*) Central Death Valley, and (*C*) Southern Death Valley with expected observed discharge variation.

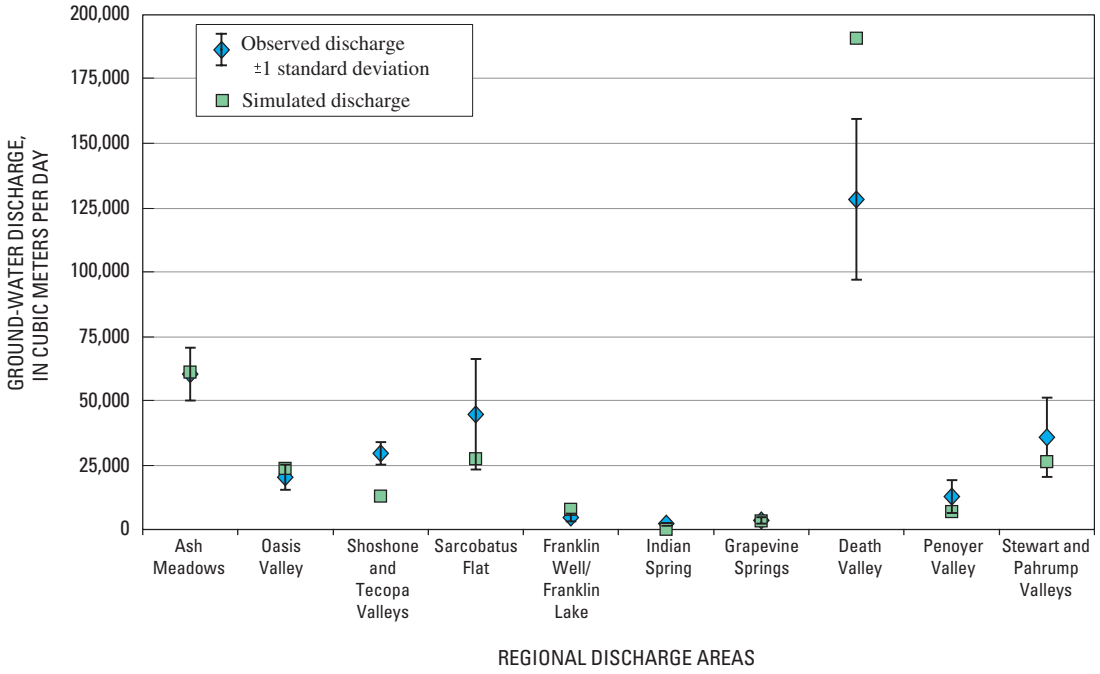

Figure F–45. Observed and simulated ground-water discharge observations by major discharge area with expected observation discharge variation.

Patterns in the spatial distribution of weighted residuals indicate a nonrandom distribution, indicating some model error (fig. F–47). In the northwestern part of the Amargosa Desert, weighted residuals are of moderate magnitude, but heads are consistently simulated lower than observations near the Bullfrog Hills and the slopes of the Funeral Mountains. Heads also are consistently simulated higher than in the northeastern arm of the Amargosa Desert and along the slopes of the southern part of the Funeral Mountains. Although a number of well-matched observations exist, weighted residuals also indicate that heads are simulated higher than observations at the northern part of Pahute Mesa and lower than observations on the southeastern part of Pahute Mesa (fig. F–47). There are four simulated head values of 2,500 m near the peak of the Spring Mountains; these simulated values are greater than observations, possibly indicating model bias. Where concentrated hydraulic-head observations are available for the remainder of the model domain, the distribution of the weighted residuals is random (fig. F–41*B*).

When plotted against simulated values, most of the weighted residuals for hydraulic heads vary randomly about a value of zero (fig. F–41*B*). However, 13 head-change weighted-residual values are greater than +8.2, which is three times the regression standard error of 2.7; 3 values are less than –8.2. Thirty-one hydraulic-head weighted-residual values are greater than 8.2; 26 values are less than –8.2. For normally distributed values, only 3 in 1,000 on average would be so different from the expected value. Here, out of about 4,900 observations, 57 are greater in absolute value than three times the standard error of the regression, with most of those being positive. Although this distribution is slightly biased, it is still largely random. Many of the head observations with large negative weighted residuals can be attributed to steep hydraulic gradients or potentially perched water levels (D'Agnese and others, 1997; D'Agnese and others, 2002). Many of the large positive weighted residuals are along the northern and southern parts of the model boundary, where considerable uncertainty exists in the hydrogeology.

Changes in Hydraulic Heads for the Transient Stress Periods

Changes in hydraulic heads for the transient stress periods were evaluated by assessing head residuals and by examining hydrographs. Weighted values of head change do not fall along a 1 to 1 line, indicating bias (fig. F–42*C*). Overall, the simulated head change is less than the observed head change, and not enough drawdown was simulated. Additionally, two outliers are located south of Beatty, Nev., where model-predicted drawdown is about 7 m, but 70 m or more of drawdown was observed. The clustering of head changes about the simulated model value of 0 is a result of generally underpredicting drawdown; many simulated head-change values are within about 5 m of observed head changes.

The simulated heads were compared with observed heads by using hydrographs from 869 of the wells in the model domain. Representative hydrographs (pl. 2) are, for the most part, grouped by wells from different pumping areas. In general, the simulated head changes match the observed head changes. Discrepancies between the simulated heads

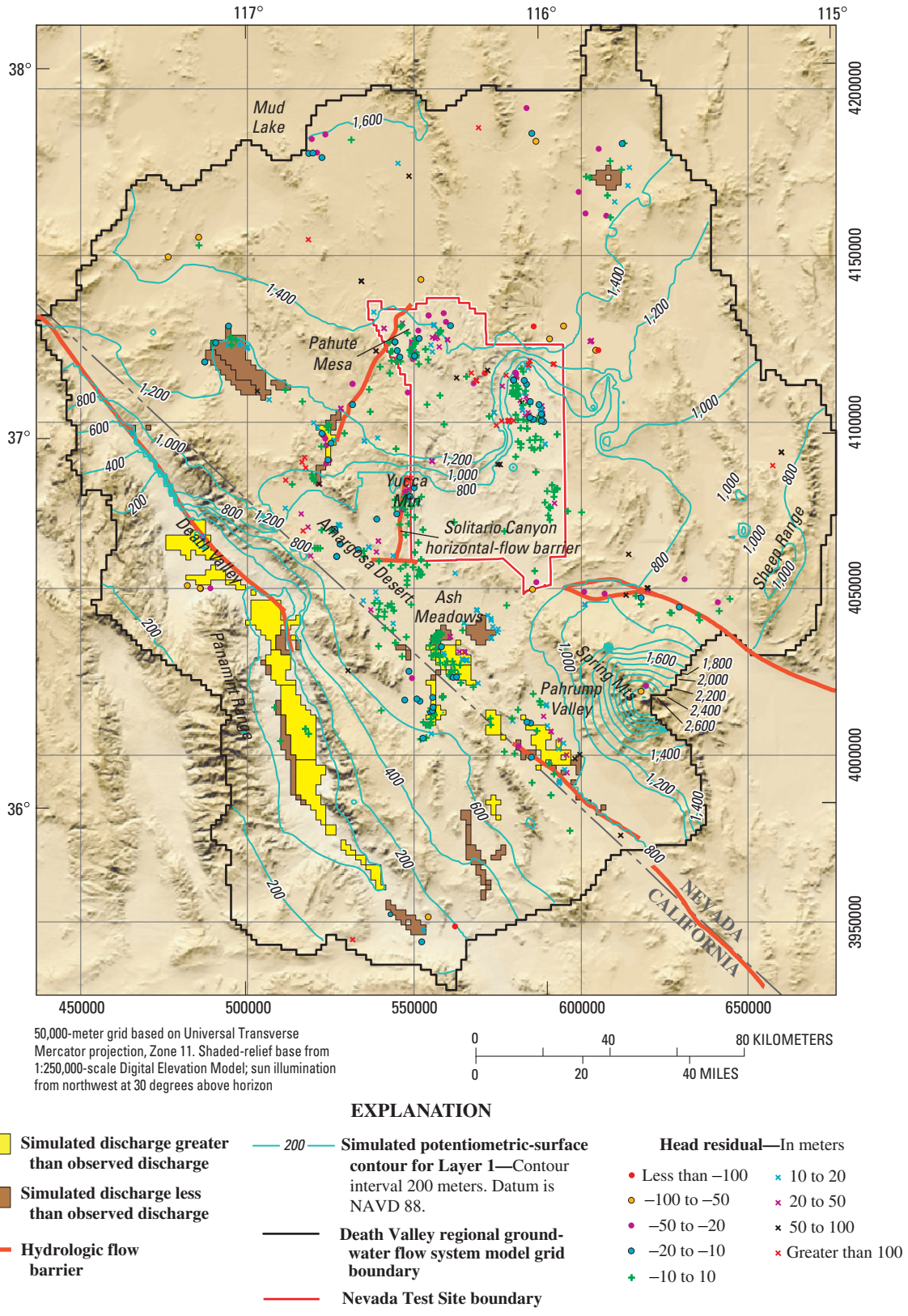

Figure F–46. Steady-state stress period hydraulic-head residuals (observed minus simulated) and simulated potentiometric surface for uppermost active model layer.

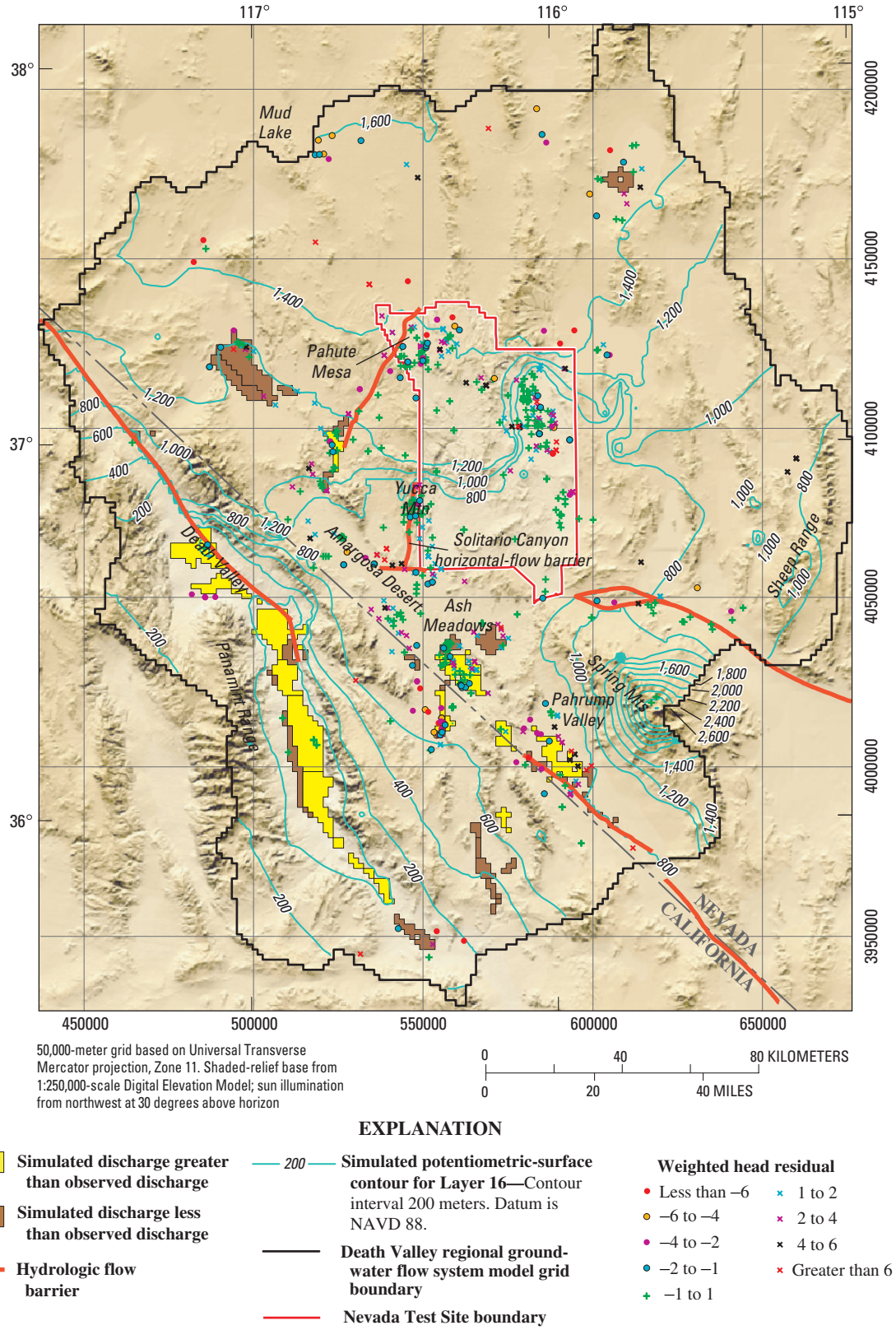

Figure F–47. Steady-state stress period hydraulic-head weighted residuals (observed minus simulated) and simulated potentiometric surface for uppermost active model layer 16.

and the observed heads may be caused, in part, by assuming that pumping is constant during each calendar year. For some areas, the match between simulated and observed values likely could be improved with better estimates of the quantity and temporal distribution of pumping.

For wells in the Amargosa Desert and Penoyer Valley, the observed heads began declining in the 1960's and 1970's, respectively (pl. 2), and these declines were generally matched by simulated heads. The hydrogeologic system at Pahrump Valley appears to be complicated as a result of large amount of pumpage over various time periods from various basin-fill units. Observed heads began to decline significantly in the 1960's and the declines continued, for most locations in Pahrump Valley, until the late 1980's. In some areas, heads are still declining, but in other areas, heads began to recover in the 1990's. Examination of the simulated hydrographs (pl. 2) shows that in some areas in Pahrump Valley these features are matched and in other areas they are not. Because of the complex hydrogeologic system in Pahrump Valley, a more detailed model would be needed to simulate head changes more accurately. The transient simulation is discussed in more detail in the "Evaluation of Hydrologically Significant Areas" section.

Normality of Weighted Residuals and Model Linearity

Linear confidence intervals on estimated parameters are valid only if the model correctly represents the system; that is, weighted residuals are normally distributed and the model is effectively linear. However, normal probability plots for the weighted residuals (not presented here) were not linear. The R^2_N statistic (Hill, 1998, p. 23) equaled 0.871, indicating that the normal probability plot is significantly nonlinear. Correlations among weighted residuals caused by the fitting of the simulated values to the observations could cause the deviation from a straight line. Model linearity was statistically tested using the modified Beale's measure (Cooley and Naff, 1990). The modified Beale's measure calculated for the transient simulation equals 212. This value indicates that the model is highly nonlinear (modified Beale's measure greater than 0.66). This lack of normality of the weighted residuals and the degree of nonlinearity of the model indicate that linear confidence intervals for parameter values may not be valid.

Evaluation of Estimated Parameter Values and Sensitivities

Most of the parameters estimated during model calibration were related to hydraulic conductivity (horizontal hydraulic conductivity, horizontal-flow barriers, drain conductances, vertical anisotropy, and depth decay). Of the 100 defined parameters, 23 were estimated in the steady-state simulation, and 32 were estimated in the transient simulation (fig. F–48 and tables F–8—F–11). The other defined parameters were not estimated because *CSS* and(or) *PCC* values indicate that there is inadequate information to estimate them. Compared to field-measured hydraulic-conductivity estimates (Belcher and others, 2001), estimated parameter values appeared realistic (figs. F–37 and F–38, tables F–8—F–11), revealing very little indication of model error.

Evaluation of Boundary Flows

Although simulated values of flow for each boundary segment (or subsegment) differ somewhat from those reported by Harrill and Bedinger (Appendix 2, this volume), except for the Silurian segment, the direction of flow is simulated accurately and the flows are generally matched well within their estimated error. For the Silurian segment, simulated flow is about 1,500 m^3/d out of the model domain, rather than an inflow of 500 m^3/d. Despite the generally low-permeability rocks along most of the western boundary, estimates indicate a potential for flow into the model domain across the Clayton, Eureka, Saline, Panamint, and, to a lesser degree, the Owlshead boundary segments (Appendix 2, this volume). The model simulates net flow greater than 1,000 m^3/d into the model domain at these segments. Net flow out of the model domain with a net flow greater than 1,000 m^3/d across the Las Vegas, Sheep Range, Pahranagat, and the Silurian boundary segments is simulated. The simulated flow out of the system at parts of the Pahranagat and Sheep Range boundary segments and the inflow across the Stone Cabin–Railroad boundary segment are much greater than estimated. These differences may result from inaccuracies in the HFM or in the boundary-flow estimates.

Evaluation of Hydrologically Significant Areas

The simulation of the conceptual hydrologic model presented in Chapter D (this volume) was evaluated in several hydrologically significant areas. These areas are: (1) the Sheep Range; (2) the Pahranagat Range; (3) northern Death Valley and Sarcobatus Flat; (4) the pumping centers of Pahrump Valley, Penoyer Valley, and the Amargosa Desert; and (5) the NTS area (including Yucca Mountain). Hydrochemical, isotopic, and thermal data (see Chapter D, this volume) were used, where possible, to help delineate the flow system and assess whether simulated flow paths were reasonable. These hydrochemical characteristics are used as qualitative information to help in the calibration of the flow model and to indicate where flow directions and magnitudes are reasonable.

Sheep Range

In the original conceptual model of the flow system, the boundary of the model was placed at the flow system boundary in the vicinity of the Sheep Range, which was assumed to coincide with the approximate trace of the Gass Peak thrust fault (fig. F–49 and Chapter D, this volume). On the basis of examination of the limited regional-potential data

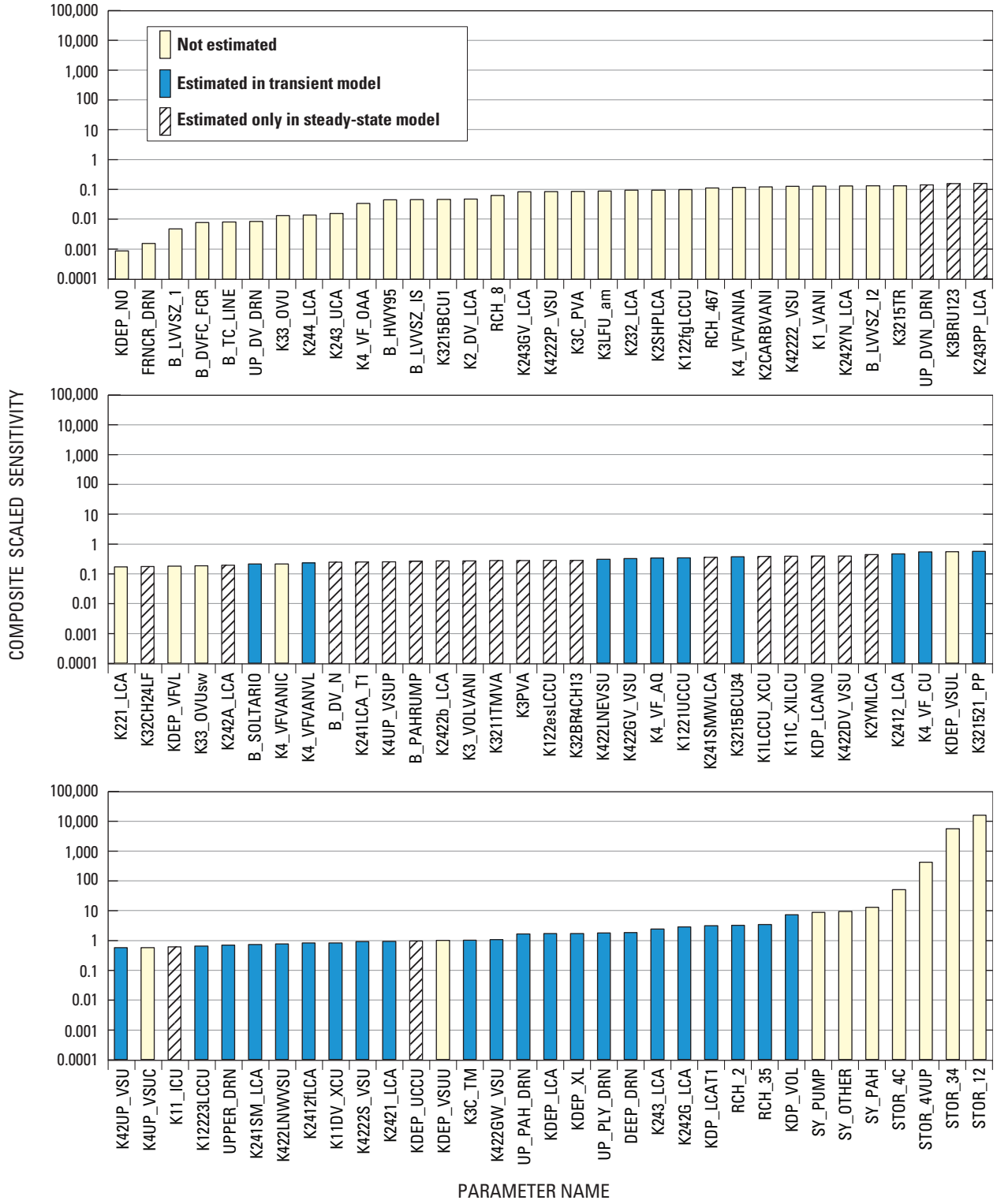

Figure F–48. Composite scaled sensitivities for all parameters. Parameter RCH_9 had a composite-sealed sensitivity of virtually zero and is not included in the figure.

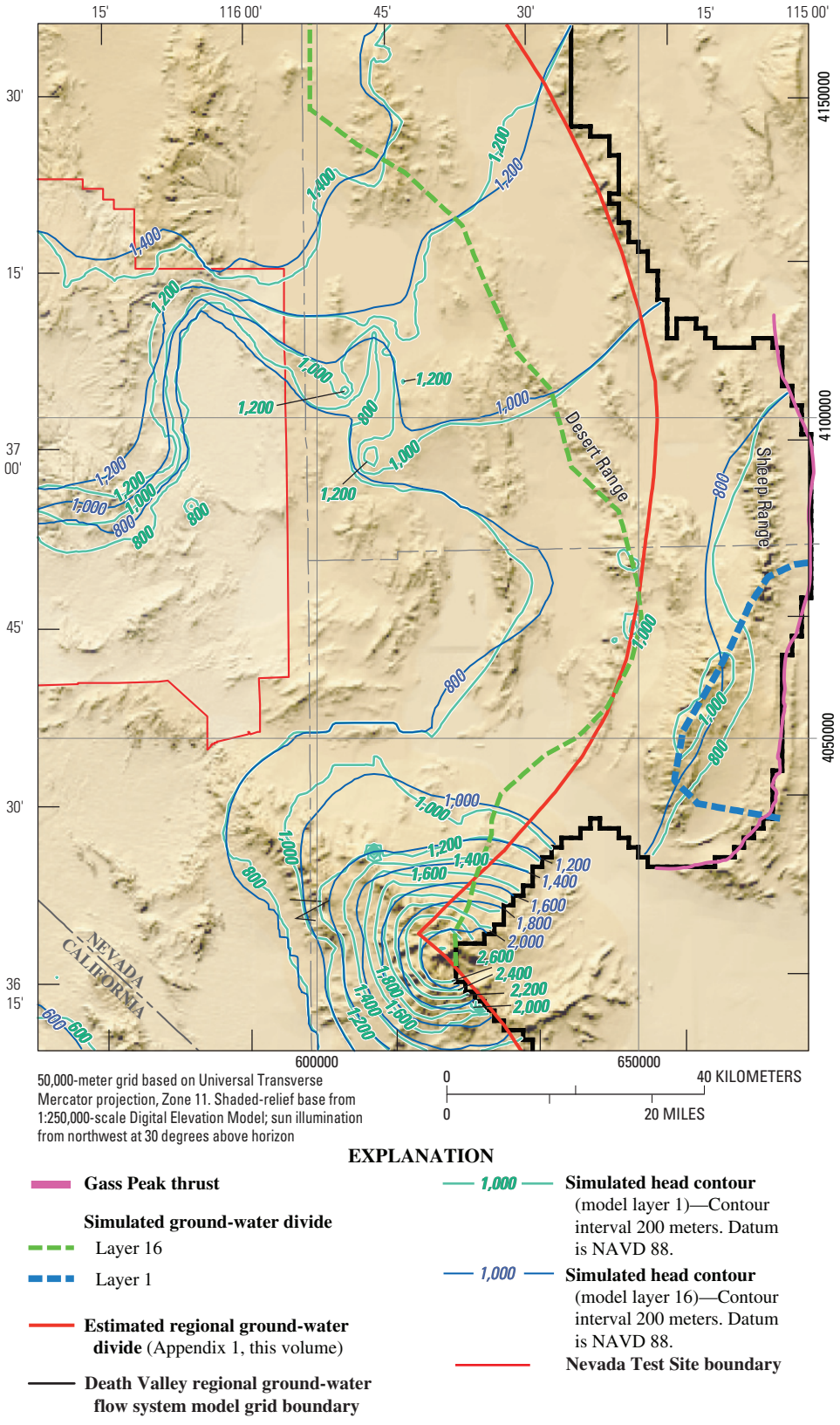

Figure F–49. Model boundary and ground-water divide near Sheep Range with simulated potentiometric surface from model layers 1 and 16.

(Appendix 1, this volume), the flow system boundary actually may be west of the model boundary in the approximate location of the Desert Range (fig. F–49 and pl. 1), and flow east of this ground-water divide would be to the Colorado River ground-water flow system. In the upper layers of the model (layer 1, for example), the location of this ground-water divide is controlled primarily by topography and the presence of recharge areas (fig. F–49). Simulated recharge on the southern Sheep Range exits the model domain to the east.

The simulated ground-water divide is not a vertical plane, and in the deeper parts of the model, the position of the divide is controlled by geology and regional hydraulic gradients. The LCCU in the upper plate of the Gass Peak thrust is modeled in the HFM (Chapter E, this volume) thinner than previous geologic interpretations (Chapter B, this volume), indicating a less effective barrier to ground-water flow. Simulated head for the lower model layers representative of the deep regional system (layer 16, for example), indicates a ground-water divide in the general area of the regional ground-water divide estimated from regional potentiometric data (fig. F–49, pl. 1, and Appendix 1). Differences in the simulated ground-water divide with depth are owing to the scarcity of head data and the relatively large simulated vertical hydraulic conductivity in this area.

Pahranagat Range

Early studies describe the Ash Meadows ground-water basin as potentially receiving ground-water flow from the Pahranagat Range (fig. A–1, and Chapter D, this volume). On the basis of more recent studies (Chapter D, this volume), little to no flow is simulated from the Pahranagat Range to Ash Meadows. An overall net outflow is simulated along the Pahranagat boundary segment. Water enters the system along the Garden-Coal boundary segment and exits along the northern part of the Pahranagat boundary segment. Flow also is simulated entering the model domain across the Pahranagat boundary segment and exiting through the Sheep Range boundary segment.

Northern Part of Death Valley and Sarcobatus Flat

Although the observed heads and spring flow and flow across the Eureka Saline boundary segment appear to be adequately simulated, discharge from drains representing ET is simulated much higher than observed (figs. F–46 and F–47). The steep hydraulic gradient required to simulate discharge to Grapevine Springs and reasonable ET rates in northern Death Valley was maintained by specifying an HFB along the northern Death Valley fault zone. Although geologically reasonable, the extremely low permeability barrier required to produce the observed discharge from Grapevine Springs resulted in simulated heads that are above land surface on the floor of Death Valley and upgradient from this fault zone. Given the current HFM (Chapter E, this volume), this feature is required to simulate discharge at Grapevine Springs.

This HFB, however, could not simulate the observed discharge at Sarcobatus Flat, even with local recharge. Inflow along the northern model boundary (Stone Cabin–Railroad and Clayton boundary segments) in excess of that estimated (Appendix 2, this volume) was required to simulate heads and observed discharge at Sarcobatus Flat. The excess inflow, the configuration of the HFM, and the constant heads specified along the Stone Cabin–Railroad boundary segment resulted in heads being simulated above land surface at Mud Lake (fig. F–46 and F–47). The simulated discharge at Sarcobatus Flat was less than observed (figs. F–44—F–47).

Pahrump Valley

Although the general trends, heads, and drawdowns are approximated on a regional scale, the DVRFS model appears to lack sufficient detail to accurately simulate ground-water flow in the complex basin-fill system of Pahrump Valley (fig. A–1 in Chapter A, this volume). Heads respond differently to pumping over short distances, so that the heads are accurately simulated in some areas of Pahrump Valley but not in others (pl. 2).

Examination of selected hydrographs for Pahrump Valley (pl. 2, HG 11–17) shows the variable heads and drawdown. In general, trends are simulated; however, spikes are not. The pumping induces hydraulic gradients that increase and decrease with changes in pumping over the simulation period (pl. 2, HG 11,12, and 14). Pumping in this area appears to decrease from the 1950's on, while pumping in other areas, often in shallower wells, increases (pl. 2, HG 11–14). Plate 2 (HG 11, 13, and 16) shows that the simulated trends are matched fairly well and most of the effects in this area are in layers 1 and 2 (pl. 2, HG 11); however, the simulated trends are subdued (HG 12). A prominent feature of HG 12 is that head observations with the highest weights are matched well, and head observations with lower weights are matched less well, indicating that the lower weights may be contributing to the subdued nature of the hydrograph. In the northern part of Pahrump Valley, wells in model layer 1 are much less affected by pumping than wells in the deeper model layers, with maximum drawdown occurring in the 1990's. Because pumping occurs mostly in the eastern and central parts of the valley, there has been little effect from pumping in the western part of the valley (pl. 2, HG 15). The effect of some of the more recent, larger pumping rates in the eastern part of the valley can be seen on the map of head change (pl. 2) and on HG 13 (pl. 2). A small amount of drawdown in the southeastern part of Pahrump Valley is indicated by a long-term water-level record (pl. 2, HG 17). The simulated heads in this area are less than observed but replicate the small drawdown over time.

In order to simulate the change in natural discharge due to pumping in the Pahrump Valley (including both ET and spring flow), three values of discharge were estimated

from various data for Bennetts and Manse Springs areas (Chapter C, this volume). The discharge observations represent that the springs went dry prior to the end of the simulation period, although ET continued (fig. F–40). Simulated discharge and discharge observations are matched relatively well from 1959 to 1961; however, discharge prior to and after this period is not simulated as accurately. Although a general trend of decreasing simulated discharge with time is evident (fig. F–40), the decrease is not at the same rate as observed. Early-time discharge observations are simulated lower than expected, and late-time observations are simulated higher than expected.

Penoyer Valley

Little is known about the hydrogeology of Penoyer Valley (fig. A–1 in Chapter A, this volume). Given that many of the drains simulating ET in the valley are dry, and the discharge rate is greatly underestimated, the drain altitudes may be simulated higher than is reasonable or the hydrogeologic conditions may not be represented correctly. Most of the wells in the Penoyer Valley are shallow and some areas are affected by drawdown. Head observations (figs. F–46 and F–47) and hydrographs (pl. 2, HG 21–23) show that heads and general trends of head change are matched where pumping does and does not occur. In most areas, heads are matched within 10 m, while in isolated areas, the unweighted head residuals reach 20 m (fig. F–46 and pl. 2). As in other areas, abrupt changes in heads shown in the hydrographs are not simulated. Although this area is adjacent to the model boundary, flow across these boundary segments does not appear to be affected by the pumping. The proximity of the constant-head boundary may also be influencing the high head residuals in this area. To match these head observations, unrealistically low hydraulic conductivity values and high specific storage values were required.

Amargosa Desert

The Amargosa Desert has two main centers of pumping, Ash Meadows and Amargosa Farms. At Ash Meadows, heads generally are matched well in the shallow model layers (layers 1–3) and generally show a small upward hydraulic gradient (pl. 2, HG 1–3 and fig. F–46). In the deeper model layers (fig. F–47), such as those representing the carbonate-rock aquifer at Devils Hole (pl. 2, HG 27), heads are not matched as well and show a small downward hydraulic gradient. Despite the poor fit of simulated and observed head at Devils Hole (pl. 2, HG 27), a small amount of drawdown can be seen in the 1970's and some recovery in late 1970's to early 1980's, simulating the hydraulic connection between the basin-fill units, where pumping is occurring, and the LCA.

Except for a few wells, very little drawdown is seen in the hydrographs (pl. 2). Because of the numerous wells in the area (fig. F–9), most completed without casing, and the simulation of the hydraulic connection between layers with the MNW package, heads appear to begin to increase in model layer 1 in the 1980's) (pl. 2, HG 1). Because of the lack of information required to define the effects of the well-bore inflow, the simulation of flow from higher heads in deeper parts of the system through inactive well bores into lower heads in shallower parts of the system may be incorrect. Drawdown from pumping in nearby wells is superimposed on this increase.

In the Amargosa Farms area, there generally is a good match of simulated to observed heads (<10-m residuals, fig. F–46; pl. 1, HG 4–9), though the match is poor for some wells (pl. 2, HG 10). On the adjacent alluvial fans sloping up to the Funeral Mountains, simulated heads are somewhat lower than observations. Heads are also less well matched in the northwest arm of the Amargosa Desert (fig. F–46, pl. 2, HG 10). Pumping rates in this northwestern area are lower than in other areas in the Amargosa Desert, resulting in less drawdown with strong upward hydraulic gradients. In most areas, the trend of head changes resulting from changes in pumping is matched reasonably well in the model (pl. 2, HG 4–10). Spikes generally are not matched well (pl. 1, HG 8), but some small head changes (pl. 2, HG 5) appear to be local effects and are matched well.

Nevada Test Site and Yucca Mountain

At the NTS, recharge and discharge areas are represented by downward and upward hydraulic gradients in a number of the deeper wells (pl. 2, HG 18–20 and 28). Some heads are simulated higher than observed values, and others are simulated lower than observed values (fig. F–46; pl. 2, HG 18–20). There has been minimal pumping at the NTS, and, as a result, little drawdown is observed in simulated hydrographs (pl. 2, HG 18–20). Fenelon (2000) describes NTS wells in which pumping effects were evident, as is shown in HGs 18 and 28 (pl. 2). More than 10 m of drawdown is measured and simulated in some wells (pl. 2, HG 28).

At Yucca Mountain, simulated hydraulic gradients are generally upward from the carbonate-rock aquifer into the volcanic rocks (pl. 2, HG 26). The potentiometric surface at and to the east of Yucca Mountain is generally flat and the simulated heads are mostly within 10 m of the observations (fig. F–46; pl. 2, HG 25 and 26). The steep hydraulic gradient at the northern end of Yucca Mountain may be caused by perched water levels (Luckey and others, 1996). Because of this possibility, head observations in wells associated with this steep hydraulic gradient were given lower weights. Because of these lower weights and the inability of the model to simulate such a steep hydraulic gradient at a regional scale, a steep hydraulic gradient is simulated, but not as steep as observed. Heads are lower than observations to the north and higher than observations to the south (fig. F–46). A moderate hydraulic gradient on the western side of Yucca Mountain, likely associated with the Solitario Canyon fault (fig. F–46), was simulated by an HFB at the location of the fault. Although some pumping has

occurred periodically for water supply and tests associated with the hydrogeologic characterization of Yucca Mountain, little drawdown is observed at a regional scale.

Model Evaluation Summary

The evaluation of the DVRFS transient model described on the preceding pages indicates that the model simulates observed values reasonably well. The three-dimensional aspects of the flow system are simulated with downward hydraulic gradients in recharge areas and upward hydraulic gradients in discharge areas. Most wells are in discharge areas and as a result, observations and hydrographs are biased to show upward hydraulic gradients.

Pumping from both shallow and deeper layers of the model is imposed early in the transient simulation. Simulation of increased pumping, mostly from the shallow layers for stress periods corresponding to the 1950's and 1980's, resulted in local drawdown cones and reversals of hydraulic gradients. Since 1998, most of the pumpage has come from ground-water storage in the system. A small amount of flow comes from a decrease in discharge at ET areas and springs (mostly in Pahrump Valley). The model underestimates this decrease in natural discharge in Pahrump Valley.

Generally, the simulated boundary flows matched the estimated boundary flows well within their estimated error. Changes in flow across the model boundary segments are negligible, indicating that the effects of pumping have not reached the model boundary.

Evaluation of model fit on the basis of weighted residuals of heads and discharges reveals one or more types of model error: (1) large positive weighted residuals for some head observations in steep hydraulic-gradient areas indicate that simulated heads in these areas are significantly lower than the observations, (2) large negative weighted residuals for ground-water discharge rates in Death Valley indicate that the simulated discharge rate is greater than the observations, (3) large positive weighted residuals for ground-water discharge rates at Sarcobatus Flat indicate that the simulated discharge is smaller than the observations, and (4) positive weighted residuals for ground-water discharge rates in Pahrump Valley in the transient simulations indicate that the simulated discharge rates are greater than the observations.

Model Improvements

The transient model is based on up-to-date geologic and hydrogeologic framework models of the regional flow system. The models represent an intensive integration and synthesis of the available hydrogeologic data and interpretations for the DVRFS.

Data and Data Analysis

The DVRFS ground-water flow model described in this report reflects the current representation of hydrogeologic and hydrologic data for the region. This current understanding affects nearly every aspect of the flow system and improves the constraints on the conceptual and numerical flow models. Improvements in data and data analysis include:

- More detailed description and delineation of the basin-fill units over the entire DVRFS model domain, particularly in the Amargosa Desert,
- Increased understanding of the volcanic-rock stratigraphy at the NTS and Yucca Mountain based on recent drilling,
- Evaluation of recharge using surface-process modeling,
- More accurate and comprehensive measurement of natural ground-water discharge (ET and spring flow),
- More complete compilation and analysis of hydraulic-head and pumpage data, especially in areas not included in previous models, and
- Evaluation of boundary inflows and outflows, resulting in a more realistic depiction of the flow system than in previous conceptual models.

Model Construction and Calibration

In addition to advances in data collection, compilation, and analysis, the ways in which these data were applied in the modeling process also represent significant advances in simulating hydrogeologic systems. For example:

- The DVRFS model simulates transient, long-term regional-scale changes in hydraulic heads and discharges that result from pumpage.
- Using the HUF package allowed the HGUs to be defined independently of model layers, linking the HFM and the flow models more directly. This linkage facilitated testing many different conceptual models.

Model Limitations

All models are based on a limited amount of data and thus are necessarily simplifications of actual systems. Model limitations are a consequence of uncertainty in three basic aspects of the model, including inadequacies or inaccuracies in (1) observations used in the model, (2) representation of geologic complexity in the HFM, and (3) representation of the ground-water flow system in the flow model. It is important to understand how these characteristics limit the use of the model.

Observation Limitations

Observations of hydraulic-head and ground-water discharge, and estimates of boundary flows, constrain model calibration through parameter estimation. Uncertainty in these observations introduces uncertainty in the results of flow-model simulations. Although head and discharge observations were thoroughly analyzed prior to and throughout calibration, there was uncertainty regarding (1) the quality of the observation data, (2) appropriateness of the hydrogeologic interpretation, and (3) the representation of observations in the flow model.

Quality of Observations

The clustering of head observations limits the flow model because it results in the overemphasis of many observations in isolated areas, thus biasing those parts of the model. Outside the Yucca Mountain, NTS, Amargosa Desert, and Pahrump Valley areas, water-level data are sparse, both spatially and temporally. A method of better distributing weights for these situations would reduce model uncertainty.

Some hydraulic-head observations used in the steady-state calibration likely are affected by pumping. Many observations in agricultural areas represent measurements made in pumping wells. Because many of the wells in the Amargosa Desert and Pahrump Valley were drilled at the start of, or after, ground-water development, it is difficult to assess which of these observations best represents prepumping conditions.

The errors in estimates of the model boundary flow also affect the accuracy of the model. Any unknown, and thus unsimulated, flow diminishes model accuracy, and improving the boundary-flow estimates can reduce model uncertainty.

Interpretation of the Observations

It is difficult to assess whether certain head observations represent the regional saturated-zone or local perched-water conditions. Areas of steep hydraulic gradient, which are important features in the regional ground-water flow system, also may be an artifact of perched water levels. The uncertainty used to weight head observations in recharge areas commonly was increased because large head residuals indicated the possibility of perched water. Decreasing the number of observations, or reducing observation weights, increased model uncertainty. Further evaluation of potentially perched water levels in these areas may help to reduce model uncertainty.

Most discharge observations were computed on the basis of vegetated areas, and it is assumed that these areas are similar to their size prior to ground-water development. In some areas, such as Pahrump Valley, this assumption may not be entirely valid because local pumping already had lowered water levels and decreased the size of the discharge areas. The uncertainty in the discharge observations increases uncertainty in the flow model.

Representation of Observations

Because of the small distance affected and comparably large grid-cell size, simulating drawdowns near wells with small pumpage rates (less than 700 m^3/d) was difficult because the cones of depression are small relative to the size of the model grid. This limitation may be resolved by creating a higher resolution model, lowering the weights on the observations, or by removing these head-change observations from the model.

The altitude assigned to drains affected the ability of the model to simulate ground-water conditions accurately. The altitude of drains used to simulate discharge through ET and spring flow likely approximates the extinction depth for all discharge areas, particularly in areas with highly variable root depth of plants and discontinuous areas of capillary fringe. Penoyer Valley is an example of a discharge area that may have a zone of fairly extensive capillary effects contributing to ET. The observed heads are lower than the drain altitudes, and the Penoyer Valley drain, or any drain with similar relative heads, will not discharge if the heads are simulated accurately.

Incised drainages and other focused discharge areas are difficult to simulate accurately at a grid resolution of 1,500 m because in many cases, the hydraulic conductivity of the HGUs at the land surface controls the simulated discharge. In situations where this methodology does not control flow, a consistent method for assigning drain conductance needs to be used.

Hydrogeologic Framework Limitations

The accuracy of the ground-water flow model depends on the accuracy of the hydrogeologic conceptual model. Limitations exist in the ground-water flow model because of the difficulties inherent in the interpretation and representation of the complex geometry and spatial variability of hydrogeologic materials and structures in both the HFM and the flow model.

Complex Geometry

Geometric complexity of hydrogeologic materials and structures is apparent throughout the model domain. One notable example is the Las Vegas Valley Shear Zone (LVVSZ). Simulation of heads in this area is limited by the current understanding of fault-system geometry and the accuracy and resolution of its representation in the HFM and in the ground-water flow model.

Similarly, the steep hydraulic gradient that extends from the Groom Range through the Belted and Eleana Ranges to Yucca Mountain and the Bullfrog Hills is inadequately simulated because of an incomplete understanding of the complex geometries in this area. However, the steep hydraulic gradient also is simulated inadequately because of simplifications inherent in the HFM and ground-water flow model construction and discretization.

Complex Spatial Variability

The spatial variability of material properties of the HGUs and structures is represented to some degree in the model (Chapter B, this volume). Incorporating these features in the flow model substantially improved the simulation; however, the model remains a significantly simplified version of reality, resulting in imperfect matching of hydraulic gradients and heads affected by detailed stratigraphy not represented in the HFM. In the ground-water flow model, the assumption of homogeneity within a given HGU or hydraulic-conductivity zone removes the potential effects of smaller scale variability. A particularly noteworthy area where poor model fit exists is in the vicinity of Oasis Valley and the Bullfrog Hills. In this area, the observed effects of hydrothermal alteration are characterized incompletely by data and inadequately represented in the HFM and the ground-water flow model. Many of the inadequacies in the simulation of heads within the SWNVF are caused in part by the underrepresentation of local-scale hydrogeologic complexities in the HFM and the ground-water flow model.

Flow Model Limitations

Three basic limitations of the flow model are inherent in its construction. These inaccuracies are in (1) representation of the physical framework, (2) representation of the hydrologic conditions, and (3) representation of time.

Representation of Physical Framework

While the 1,500-m resolution of the flow model grid is appropriate to represent regional-scale conditions, higher resolution would improve simulation accuracy, particularly in areas of geologic complexity. The large grid cells tend to generalize important local-scale complexities that affect regional hydrologic conditions. To represent more local dynamics, smaller grid cells throughout the model (or local refinement around selected features or in critical areas in the model domain) would be required.

Representation of Hydrologic Conditions

The hydrologic conditions represented by the model are expressed as boundary conditions and include recharge, lateral boundary flows, discharge from ET and springs, and pumpage. Of these boundary conditions, the most significant is recharge. The main limitation in the representation of recharge is the inaccurate estimation of net infiltration that likely is owing in large part to the assumption that net infiltration results in regional recharge. The net-infiltration model likely overestimates recharge in many parts of the model domain because it is assumed that all infiltrating water that passes the root zone ultimately reaches the water table. This assumption ignores the possibility that infiltrating water could be intercepted and either diverted or perched by a lower permeability layer in the unsaturated zone, or the possibility of deep evaporation from the unsaturated zone. This limitation may be resolved by including in the flow model a means to account for deep, unsaturated zone processes that may act to reduce or redistribute infiltrating water.

Limitations in the definition of lateral boundary flow are the result of incomplete understanding of natural conditions. Because very little data exist in the areas defined as lateral flow-system boundary segments, all aspects of the assigned boundary conditions are poorly known. Despite these uncertainties, the data used to characterize these boundary flows have been thoroughly analyzed for this model. The model does not simulate the complex process of ET but accounts for the ground-water discharge attributed to ET through use of the Drain package for MODFLOW-2000. ET by native vegetation was studied extensively. Future revisions of the DVRFS model might be improved by using a more complex ET package instead of the Drain package. This package could incorporate spatially varying parameters to simulate direct recharge, soil moisture, and vegetative growth.

Representation of Time

The year-long stress periods simulated in the model limit its temporal applicability to dynamics that change over at least several years. Simulation of seasonal dynamics using shorter stress periods could be advantageous to account for the seasonal nature of irrigation pumpage. Such a simulation would require seasonal definition of hydrologic conditions.

Appropriate Uses of the Model

Because the DVRFS model was constructed to simulate regional-scale ground-water flow, it can be used to answer questions regarding ground-water flow issues at that scale. For example, interactions can be considered between hydraulic heads, discharge, pumping, and flow direction and magnitude on a regional scale.

The model can provide boundary conditions for the development of local-scale models, such as those being developed by the Department of Energy for both the NNSA/NSO and ORD programs. Consistency between regional and local models must be ensured. Advances in linking regional- and local-scale models may allow for simultaneous calibration and uncertainty analysis. Although regional scale by design, the DVRFS model includes many local-scale features and site-specific data. Local features include facies changes and pumpage from one or a few wells. In some circumstances the model could be used to evaluate the regional consequences of such local features. Yet, some regional consequences and all local consequences would be evaluated most effectively using local-scale models in combination with simulations from the regional model.

The model can be used to evaluate alternative conceptualizations of the hydrogeology that are likely to have a regional effect. These might include the effects of increased recharge caused by climate change, different interpretations of the extent or offset of faults, or other conceptual models of depositional environments that would affect the spatial variation of hydraulic properties.

The model also can be used to provide insight about contaminant transport. Flow direction and magnitude are appropriately represented using particle tracking methods as long as the particle paths are interpreted to represent regional, not local, conditions. The model may be a useful tool for evaluating advective-transport flow paths that are at least several times longer than the length of a 1,500-m model cell (Hill and others 2001; Tiedeman and others, 2003).

Increased urbanization in southern Nevada necessitates the development of ground-water resources. The model can be used for examining the effects of continued or increased pumpage on the regional ground-water flow system to effectively manage ground-water resources within conflicting land-use management policies.

Summary

The Death Valley regional ground-water flow system was simulated by a three-dimensional (3D) model that incorporates a nonlinear least-squares regression technique to estimate aquifer parameters. The model was constructed with MODFLOW-2000, a version of the U.S. Geological Survey 3D, finite-difference, modular ground-water flow model in which nonlinear regression may be used to estimate model parameters that result in the best fit to measured heads and discharges.

The model consists of 16 layers, on a finite-difference grid of 194 rows and 160 columns, and uniform, square model cells with a dimension of 1,500 meters (m) on each side. Model layers are simulated under confined flow conditions, so that the top of each layer and its thickness are defined. Although the top of the actual flow system is unconfined, the model accounts for the position of the simulated potentiometric surface in the top model layer to account for the thickness of the top layer and approximate unconfined flow conditions. Prepumping conditions were used as the initial conditions for the transient-state calibration of the model. Transmissivity is temporally constant and is spatially defined by hydrogeologic units (HGUs) and zones within some of these units. Storage properties were constant in time.

The model design was based on a 3D hydrogeologic framework model (HFM) that defines the physical geometry and composition of the surface and subsurface materials of 27 HGUs through which ground water flows. The HFM defines the geometry of the HGUs in the model domain (the area inside the model boundary).

Several conceptual models were evaluated during calibration to test the validity of various interpretations about the flow system. The evaluation focused on testing alternative hypotheses concerning (1) the location and type of flow system boundaries, (2) the definition of recharge areas, and (3) variations in interpretation of the hydrogeologic framework. For each conceptual model, a new set of parameters was estimated, and the resulting simulated hydraulic heads, drawdowns, ground-water discharges, and boundary flows were compared to observed values. Only those conceptual model changes contributing to a significant improvement in model fit were retained in the final calibrated model.

Ground-water flow into the model is from the simulation of infiltration of direct precipitation (recharge) and, to a lesser extent, from the simulation inflow across the model boundary. The distribution of simulated recharge varies spatially but is held at a constant rate for the entire simulation period. Ground-water flow out of the model primarily is through simulated ET, spring flow and pumping, and, to a lesser extent, by outflow across the model boundary. Observations of the combined discharge by ET and spring flow and estimated boundary flows were used to calibrate the model.

Boundary flows into and out of the model domain were simulated using head-dependent boundaries that were assigned the regional potentiometric surface altitude. Because previous models of the system generally used no-flow boundaries, the representation of inflow and outflow across the model boundary from adjacent systems are significantly different. In particular, ground-water flow from the north is simulated to sustain heads in the northern parts of the Nevada Test Site and, in particular, discharge around Sarcobatus Flat.

The final calibration was evaluated to assess the accuracy of simulated results by comparing measured and expected values with simulated values. The fit of simulated heads to observed hydraulic heads is generally good (residuals with absolute values less than 10 m) in most areas of nearly flat hydraulic gradients, and moderate (residuals with absolute values of 10 to 20 m) in the remainder of the areas of nearly flat hydraulic gradients. The poorest fit of simulated heads to observed hydraulic heads (residuals with absolute values greater than 20 m) is in steep hydraulic-gradient areas in the vicinity of Indian Springs, western Yucca Flat, and the southern Bullfrog Hills. Most of these inaccuracies can be attributed to (1) insufficient representation of the hydrogeology in the HFM, (2) misinterpretation of water levels, and (3) model error associated with grid cell size.

Ground-water discharge residuals are fairly random, with as many areas in which simulated discharges are less than observed discharges as areas in which simulated discharges are greater than observed. The largest unweighted ground-water discharge residuals are in Death Valley and Sarcobatus Flat (northeastern area). The two major discharge areas that contribute the largest volumetric error to the model are the Shoshone/Tecopa area and Death Valley. Positive

weighted residuals were computed in transient simulations of the Pahrump Valley that may indicate a poor definition of hydraulic properties and(or) discharge estimates, especially near Bennetts Spring.

Parameter values estimated by the regression analyses were reasonable—that is, within the range of expected values. As with any model, uncertainties and errors remain, but this model is considered an improvement on previous representations of the flow system.

The model is appropriate for evaluation of regional-scale processes. These include the assessment of boundary conditions of local-scale models, the evaluation of alternative conceptual models, the approximation of aspects of regional-scale advective transport of contaminants, and the analysis of the consequences of changed system stresses, such as those that would be imposed on the system by increasing pumpage.

Inherent limitations result from uncertainty in three basic aspects of the model: inadequacies or inaccuracies in observations used in the model, in the representation of geologic complexity in the HFM, and representation of the ground-water flow system in the flow model. It is important to understand how these characteristics limit the use of the model. These basic aspects of the model are represented at a regional scale, and the use of the model to address regional-scale issues or questions is the most appropriate use of the model.

References Cited

Anderman, E.R., and Hill, M.C., 2000, MODFLOW-2000, The U.S. Geological Survey modular ground-water flow model—Documentation of the hydrogeologic-unit flow (HUF) package: U.S. Geological Survey Open-File Report 00–342, 89 p.

Anderman, E.R., and Hill, M.C., 2003, MODFLOW-2000, The U.S. Geological Survey modular ground-water flow model—Three additions to the hydrogeologic-unit flow (HUF) package—Alternative storage for the uppermost active cells (STYP parameter type), flows in hydrogeologic units, and the hydraulic conductivity depth-dependence (KDEP) capability: U.S. Geological Survey Open-File Report 03–347, 36 p. Accessed April 14, 2004, at *http://water.usgs.gov/nrp/gwsoftware/modflow2000/modflow2000.html*

Anderman, E.R., Hill, M.C., and Poeter, E.P., 1996, Two-dimensional advective transport in ground-water flow parameter estimation: Ground Water, v. 34, no. 6, p. 1001–1009.

Anderson, M.P., and Woessner, W.W., 1992, Applied ground-water modeling—Simulation of flow and advective transport: San Diego, Calif., Academic Press, Inc., 381 p.

Bard, Jonathon, 1974, Nonlinear parameter estimation: New York, Academic Elsevier, 476 p.

Bedinger, M.S., Langer, W.H., and Reed, J.E., 1989, Ground-water hydrology, *in* Bedinger, M.S., Sargent, K.A., and Langer, W.H., eds., Studies of geology and hydrology in the Basin and Range Province, southwestern United States, for isolation of high-level radioactive waste—Characterization of the Death Valley region, Nevada and California: U.S. Geological Survey Professional Paper 1370–F, p. 28–35.

Belcher, W.R., Elliott, P.E., and Geldon, A.L., 2001, Hydraulic-property estimates for use with a transient ground-water flow model for the Death Valley regional ground-water flow system, Nevada and California: U.S. Geological Survey Water-Resources Investigations Report 01–4210, 28 p., accessed on September 1, 2004 at *http://water.usgs.gov/pubs/wri/wri014210/*

Cooley, R.L., and Naff, R.L., 1990, Regression modeling of ground-water flow: U.S. Geological Survey Techniques of Water-Resources Investigations, book 3, chap. B4, 232 p.

D'Agnese, F.A., Faunt, C.C., Turner, A.K., and Hill, M.C., 1997, Hydrogeologic evaluation and numerical simulation of the Death Valley regional ground-water flow system, Nevada and California: U.S. Geological Survey Water-Resources Investigations Report 96–4300, 124 p.

D'Agnese, F.A., Faunt, C.C., and Turner, A.K., 1998, An estimated potentiometric surface of the Death Valley region, Nevada and California, using geographic information systems and automated techniques: U.S. Geological Survey Water-Resources Investigations Report 97–4052, 15 p., 1 plate.

D'Agnese, F.A., O'Brien, G.M., Faunt, C.C., Belcher, W.R., and San Juan, Carma, 2002, A three-dimensional numerical model of prepumping conditions in the Death Valley regional ground-water flow system, Nevada and California: U.S. Geological Survey Water-Resources Investigations Report 02–4102, 114 p.

DeMeo, G.A., Laczniak, R.J., Boyd, R.A., Smith, J.L., and Nylund, W.E., 2003, Estimated ground-water discharge by evapotranspiration from Death Valley, California, 1997–2001: U.S. Geological Survey Water-Resources Investigations Report 03–4254, 27 p.

Fenelon, J.M., 2000, Quality assurance and analysis of water levels in wells on Pahute Mesa and vicinity, Nevada Test Site, Nye County, Nevada: U.S. Geological Survey Water-Resources Investigations Report 00–4014, 68 p.

Grasso, D.N., 1996, Hydrology of modern and late Holocene lakes, Death Valley, California: U.S. Geological Survey Water-Resources Investigations Report 95–4237, 53 p.

Halford, K.J., and Hanson, R.T., 2002, User guide for the drawdown-limited, multi-node well (MNW) package for the U.S. Geological Survey's modular three-dimensional finite-difference ground-water flow model, versions MODFLOW-96 and MODFLOW-2000: U.S. Geological Survey Open-File Report 02–293, 33 p.

Harbaugh, J.W., Banta, E.R., Hill, M.C., and McDonald, M.G., 2000, MODFLOW-2000, The U.S. Geological Survey's modular ground-water flow model—User guide to modularization concepts and the ground-water flow process: U.S. Geological Survey Open-File Report 00–92, 121 p.

Hevesi, J.A., Flint, A.L., and Flint, L.E., 2003, Simulation of net infiltration and potential recharge using a distributed parameter watershed model of the Death Valley region, Nevada and California: U.S. Geological Survey Water-Resources Investigations Report 03–4090, 91 p.

Hill, M.C., 1998, Methods and guidelines for effective model calibration: U.S. Geological Survey Water-Resources Investigations Report 98–4005, 90 p.

Hill, M.C., Banta, E.R., Harbaugh, A.W., and Anderman, E.R., 2000, MODFLOW-2000, The U.S. Geological Survey's modular ground-water flow model—User guide to the observation, sensitivity, and parameter-estimation procedures and three post-processing programs: U.S. Geological Survey Open-File Report 00–184, 209 p., accessed September 1, 2004, at *http://water.usgs.gov/nrp/gwsoftware/modflow2000/modflow2000.html*

Hill, M.C., Cooley, R.L., and Pollock, D.W., 1998, A controlled experiment in ground-water flow model calibration: Ground Water, v. 36, no. 3, p. 520–535.

Hill, M.C., Ely, M.D., Tiedeman, C.R., O'Brien, G.M., D'Agnese, F.A., and Faunt, C.C., 2001, Preliminary evaluation of the importance of existing hydraulic-head observation locations to advective-transport predictions, Death Valley regional flow system, California and Nevada: U.S. Geological Survey Water-Resources Investigations Report 00–4282, 82 p., accessed September 1, 2004, at *http://water.usgs.gov/pubs/wri/wri004282/*

Hill, M.C., and Tiedeman, C.R, 2003, Weighting observations in the context of calibrating ground-water models, *in* Kovar, Karel, and Zbynek, Hrkal, eds., Calibration and reliability in groundwater modeling, a few steps closer to reality: International Association Hydrological Sciences Publication 277, p. 196–203.

Hsieh, P.A., and Freckleton, J.R., 1993, Documentation of a computer program to simulate horizontal-flow barriers using the U.S. Geological Survey modular three-dimensional finite difference ground-water flow model: U.S. Geological Survey Open-File Report 92–477, 32 p.

IT Corporation, 1996, Underground Test Area subproject, Phase I data analysis task, volume IV, Hydrologic parameter data documentation package: Report ITLV/10972–181 prepared for the U.S. Department of Energy, 8 volumes, various pagination.

Laczniak, R.J., Smith, J.L., Elliott, P.E., DeMeo, G.A., Chatigyn, M.A., and Roemer, G.J., 2001, Ground-water discharge determined from estimates of evapotranspiration, Death Valley regional flow system, Nevada and California: U.S. Geological Survey Water-Resources Investigations Report 01–4195, 51 p.

Luckey, R.R., Tucci, Patrick, Faunt, C.C., Ervin, E.M., Steinkampf, W.C., D'Agnese, F.A., and Patterson, G.L., 1996, Status of understanding of the saturated-zone ground-water flow system at Yucca Mountain, Nevada as of 1995: U.S. Geological Survey Water-Resources Investigations Report 96–4077, 71 p.

Miller, G.A., 1977, Appraisal of the water resources of Death Valley, California-Nevada: U.S. Geological Survey Open-File Report 77–728, 68 p.

Moreo, M.T., Halford, K.J., La Camera, R.J., and Laczniak, R.J., 2003, Estimated ground-water withdrawals from the Death Valley regional flow system, 1913–1998, Nevada and California: U.S. Geological Survey Water-Resources Investigations Report 03–4245, 28 p.

Poeter, E.P. and Hill, M.C., 1997, Inverse modeling, a necessary next step in ground-water modeling: Ground Water, v. 35, no. 2, p. 250–260.

Potter, C.J., Sweetkind, D.S., Dickerson, R.P., Kilgore, M.L., 2002, Hydrostructural maps of the Death Valley regional flow system, Nevada and California: U.S. Geological Survey Miscellaneous Field Studies MF–2372, 2 sheets, 1:250,000 scale, 14 pages of explanatory text.

Prudic, D.E., Harrill, J.R., and Burbey, T.J., 1995, Conceptual evaluation of regional ground-water flow in the carbonate-rock province of the Great Basin, Nevada, Utah, and adjacent States: U.S. Geological Survey Professional Paper 1409–D, 102 p.

Rantz, S.E. (compiler), 1982, Measurement and computation of stream flow: U.S. Geological Survey Water-Supply Paper 2175, v. 1, p. 181–183.

Reiner, S.R., Laczniak, R.J., DeMeo, G.A., Smith, J.L., Elliott, P.E., Nylund, W.E., and Fridrich, C.J., 2002, Ground-water discharge determined from measurements of evapotranspiration, other available hydrologic components, and shallow water-level changes, Oasis Valley, Nye County, Nevada: U.S. Geological Survey Water-Resources Investigations Report 01–4239, 65 p.

Schaefer, D.H., and Harrill, J.R., 1995, Simulated effects of proposed ground-water pumping in 17 basins of east-central and southern Nevada: U.S. Geological Survey Water-Resources Investigations Report 95–4173, 71 p.

Sweetkind, D.S., and White, D.K, 2001, Facies analysis of Late Proterozoic through Lower Cambrian clastic rocks of the Death Valley regional ground-water system and surrounding areas, Nevada and California: U.S. Geological Survey Open-File Report 01–351, 13 p.

Thomas, J.M., Carlton, S.M., and Hines, L.B., 1989, Ground-water flow and simulated response to selected developmental alternatives in Smith Creek Valley, a hydrologically closed basin in Lander County, Nevada: U.S. Geological Survey Professional Paper 1409–E, 57 p.

Tiedeman, C.R., Hill, M.C., D'Agnese, F.A., and Faunt, C.C., 2003, Methods for using ground-water model predictions to guide hydrogeologic data collection with application to the Death Valley regional groundwater flow system: Water Resources Research, v. 39, no. 1, p. 5–1 to 5–17.

Van Denburgh, A.S., and Rush, F.E., 1974, Water-resources appraisal of Railroad and Penoyer Valleys, east-central Nevada: Nevada Department of Conservation and Natural Resources Ground-Water Resources—Reconnaissance Series Report 60, 61 p.

Waddell, R.K., 1982, Two-dimensional, steady-state model of ground-water flow, Nevada Test site and vicinity, Nevada-California: U.S. Geological Survey Water-Resources Investigations Report 84–4267, 72 p.